2009-09

Ocean surface wave transformation over a sandy sea bed

Coll Florit, Guillermo.

Monterey, California. Naval Postgraduate School

NAVAL POSTGRADUATE SCHOOL

MONTEREY, CALIFORNIA

THESIS

OCEAN SURFACE WAVE TRANSFORMATION OVER A SANDY SEA BED

by

Guillermo Coll Florit

September 2009

Thesis Advisor:	Thomas H.C. Herbers
Second Reader:	Jamie MacMahan

Approved for public release; distribution unlimited

THIS PAGE INTENTIONALLY LEFT BLANK

REPORT DOCUMENTATION PAGE		Form Approved OMB No. 0704-0188

1. AGENCY USE ONLY *(Leave blank)*	2. REPORT DATE September 2009	3. REPORT TYPE AND DATES COVERED Master's Thesis

4. TITLE AND SUBTITLE Ocean Surface Wave Transformation Over a Sandy Sea Bed	5. FUNDING NUMBERS
6. AUTHOR(S) Guillermo Coll Florit	
7. PERFORMING ORGANIZATION NAME(S) AND ADDRESS(ES) Naval Postgraduate School Monterey, CA 93943-5000	8. PERFORMING ORGANIZATION REPORT NUMBER
9. SPONSORING /MONITORING AGENCY NAME(S) AND ADDRESS(ES) N/A	10. SPONSORING/MONITORING AGENCY REPORT NUMBER

11. SUPPLEMENTARY NOTES The views expressed in this thesis are those of the author and do not reflect the official policy or position of the Department of Defense or the U.S. Government.

12a. DISTRIBUTION / AVAILABILITY STATEMENT Approved for public release; distribution is unlimited	12b. DISTRIBUTION CODE

13. ABSTRACT (maximum 200 words)

Projecting naval forces in littoral areas requires a thorough understanding of the environmental processes that take place in those areas, especially ocean wave evolution, and the associated surf and wave-driven currents. The transformation of wave spectra in coastal environments is predicted with numerical models that include the effects of refraction, nonlinear wave-wave interactions, and parameterizations of wave breaking and bottom friction. This thesis presents a comparison between a new field data set and model predictions of wave transformation in shallow water. An array of 16 wave-measuring instruments was deployed outside the surf zone on the sandy sea bed of Martha's Vineyard's inner continental shelf in the fall of 2007. Data from these instruments are analyzed and the performance of the spectral wave prediction model SWAN (Simulating WAves Nearshore) is tested against the observations.

The observations generally show gradual wave decay towards the shore with a reduction of as much as 15% of the incident wave height across only 4 km of continental shelf. Wave height variability is observed in both the cross-shore and the alongshore directions, suggesting that the effect of bottom processes on wave energy is two-dimensional. Comparisons of these observations with SWAN model predictions show that both bottom friction and refraction play a dominant role in the wave energy transformation outside the surf zone. Overall, the spectral wave decay is handled well by SWAN with any of the bottom friction parameterizations activated, including the widely used JONSWAP (Hasselmann et al., 1973) empirical parameterization. Deactivating bottom friction in SWAN yields a slight overprediction of nearshore wave heights.

14. SUBJECT TERMS Ocean waves, energy spectrum, SWAN, numerical prediction models, refraction	15. NUMBER OF PAGES 79
	16. PRICE CODE

17. SECURITY CLASSIFICATION OF REPORT	18. SECURITY CLASSIFICATION OF THIS PAGE	19. SECURITY CLASSIFICATION OF ABSTRACT	20. LIMITATION OF ABSTRACT
Unclassified	Unclassified	Unclassified	UU

NSN 7540-01-280-5500 Standard Form 298 (Rev. 8-98)
Prescribed by ANSI Std. Z39.18

THIS PAGE INTENTIONALLY LEFT BLANK

Approved for public release; distribution is unlimited

OCEAN SURFACE WAVE TRANSFORMATION OVER A SANDY SEA BED

Guillermo Coll Florit
Lieutenant Commander, Spanish Navy
Spanish Naval Academy, 1995
Military Geodesist, Spanish Army Geodesy School, 2002

Submitted in partial fulfillment of the
requirements for the degree of

MASTER OF SCIENCE IN METEOROLOGY AND PHYSICAL OCEANOGRAPHY

from the

NAVAL POSTGRADUATE SCHOOL
September 2009

Author: Guillermo Coll Florit

Approved by: Thomas H.C. Herbers
Thesis Advisor

Jamie MacMahan
Second Reader

Jeffrey Paduan
Chairman, Department of Oceanography

THIS PAGE INTENTIONALLY LEFT BLANK

ABSTRACT

Projecting naval forces in littoral areas requires a thorough understanding of the environmental processes that take place in those areas, especially ocean wave evolution, and the associated surf and wave-driven currents. The transformation of wave spectra in coastal environments is predicted with numerical models that include the effects of refraction, nonlinear wave-wave interactions, and parameterizations of wave breaking and bottom friction. This thesis presents a comparison between a new field data set and model predictions of wave transformation in shallow water. An array of 16 wave-measuring instruments was deployed outside the surf zone on the sandy sea bed of Martha's Vineyard's inner continental shelf in the fall of 2007. Data from these instruments are analyzed and the performance of the spectral wave prediction model SWAN (Simulating WAves Nearshore) is tested against the observations.

The observations generally show gradual wave decay towards the shore with a reduction of as much as 15% of the incident wave height across only 4 km of continental shelf. Wave height variability is observed in both the cross-shore and the alongshore directions, suggesting that the effect of bottom processes on wave energy is two-dimensional. Comparisons of these observations with SWAN model predictions show that both bottom friction and refraction play a dominant role in the wave energy transformation outside the surf zone. Overall, the spectral wave decay is handled well by SWAN with any of the bottom friction parameterizations activated, including the widely used JONSWAP (Hasselmann et al., 1973) empirical parameterization. Deactivating bottom friction in SWAN yields a slight overprediction of nearshore wave heights.

THIS PAGE INTENTIONALLY LEFT BLANK

TABLE OF CONTENTS

THIS PAGE INTENTIONALLY LEFT BLANK

LIST OF FIGURES

THIS PAGE INTENTIONALLY LEFT BLANK

LIST OF TABLES

THIS PAGE INTENTIONALLY LEFT BLANK

ACKNOWLEDGMENTS

I would like to give thanks to my advisor, Professor T.H.C. Herbers, for helping me compose this thesis. I know it has been extra work for him to review my English writing. From his editing, I have learned a lot. I also want to thank professor Jamie MacMahan for being my second reader, and Mr. Paul Jessen for helping me with complex MATLAB programming.

I really appreciate all the knowledge that the members of the NPS Faculty of the Oceanography and Meteorology Departments have transmitted to me in their classes. I am sure that what I have learned from them will help me a lot in my future assignments in the Spanish Navy.

Finally, I would like to specially thank my lovely wife Cristina who, with a lot of patience, has supported me to complete the METOC Master of Science at NPS. Both she and I are very grateful to the people of the nice city of Monterey, and will always remember our stay here.

THIS PAGE INTENTIONALLY LEFT BLANK

I. INTRODUCTION

A. MOTIVATION AND OBJECTIVE

Modern naval operations demand consistent and precise Meteorological and Oceanographic (METOC) support in order for the naval forces to accomplish their required tasks effectively and safely. Commanders can exploit reliable METOC information to optimize the planning, execution, and support of specific naval operations. The failure to provide accurate METOC information for a mission can cost lives and waste resources.

Among the many types of naval operations that rely on METOC support, is the projection of assets on coastal areas. Amphibious landings and evacuation operations are two clear examples of tasks that need to be performed in the coastal environment. This requires a thorough understanding of the environmental processes that occur in such areas. The wave field transformation in shallow water is especially important because large waves can create hazardous conditions for the navigation of small vessels through coastal waters. Accurate predictions of the coastal wave field are often critical to the success of littoral naval operations.

Not only the naval forces are interested in predicting coastal wave conditions, but also many other communities such as oceanographers, coastal engineers, and even water sports practitioners. The nearshore wave climate is especially important for the prediction and mitigation of coastal erosion.

Research institutions worldwide have been carrying out studies in order to better understand the physics of wave transformation in shallow water and improve the performance of operational wave prediction models. Wave prediction in coastal environments is a challenging task because waves are affected by many processes, including scattering by sea floor topography, strong nonlinear interactions, wave breaking, and bottom friction. Several of these processes are

poorly understood and current wave prediction models rely on empirical parameterizations that have not been well tested owing primarily to a lack of field observations.

This thesis analyzes a large new set of wave observations recorded for two months in 2007, across the inner continental shelf of the island of Martha's Vineyard (Massachusetts). The results of these observations are compared with predictions from the numerical model SWAN (Simulating WAves Nearshore).

The goal of this thesis is twofold:

To better understand the processes that cause wave energy dissipation in shallow water.

To evaluate the performance of the widely used operational wave prediction model SWAN.

The thesis is structured in six chapters. Chapter I provides motivation for the research, a background on wave transformation and energy dissipation mechanisms, and a review of previous experiments on wave transformation over continental shelves that are considered to be relevant to this study. Chapter II describes the field experiment and the instruments used to measure waves. In Chapter III the analysis procedures of the field data are described. The SWAN model is introduced in Chapter IV. A general description is given as well as the details of the model implementation for this experiment. In Chapter V the wave observations are compared with numerical model predictions. In this chapter, selected case studies and a statistical summary are presented. Finally, the summary and conclusions of this thesis are given in Chapter VI.

B. WAVE TRANSFORMATION BACKGROUND

A detailed review of theories for the generation of waves by wind and their evolution in the open ocean and coastal waters can be found in Komen et al. (1994) or Holthuijsen (2007). Here, a brief summary is given of the main processes that affect waves from their generation through propagation over long

distances to their dissipation on beaches. The array of wave-measuring instruments used in this thesis was deployed on the inner continental shelf, outside the surf zone, where the dominant wave decay mechanism is expected to be bottom friction. Therefore, focus on this process is given in a separate section.

1. Wave Generation and Evolution

Among the many types of ocean waves that can exist, the most common ones are the wind waves. As their name indicates, these are waves generated by the interaction of the wind with the surface of the ocean. The physical mechanisms that result in the generation of waves are complex and were not understood until the 1950s, when Phillips (1957) and Miles (1957) proposed theories that are now widely accepted. Phillips stated that waves are developed initially by turbulent fluctuations in the atmospheric pressure exerted against the sea surface. Miles hypothesized that the observed rapid exponential growth of waves following that initial development is caused by a feedback mechanism, in which the waves perturb the airflow and the airflow perturbs the waves. The initial theories of Phillips and Miles were later extended by Hasselmann (1962) who proposed that nonlinear interactions between waves transfer energy to lower and higher frequency components that contribute to the wave spectral development. The influence of the wind, however, cannot cause an infinite wave growth, and indeed the size of the observed waves is limited. In an attempt to explain the limited wave size, Phillips (1958) suggested that wave breaking or “whitecapping” causes a rate of dissipation that balances the wind input. As a result, wind waves stop growing and reach a certain equilibrium.

The primary factors that determine wave development by the wind are the average wind speed, the length of time during which the wind is blowing (duration), and the distance over which the wind blows (fetch). The combination of these factors will produce waves of different heights. The larger the values of these factors the larger the wave heights. The wave development by the wind

takes place within the so-called generation area. Since the turbulent wind in the marine boundary layer is chaotic in direction and speed, the character of the waves that will be formed will also be chaotic. Within the generation area, wave-wave interactions and wave breaking (whitecapping) will create a broad spectrum of wave heights and directions. Actively generated waves are often called *sea waves*. “Sea waves are irregular, chaotic, short-crested, mountainous, and unpredictable” (Pierson et al., 1955, p. 26).

Outside the generation area, waves become more regular and move in trains of similar period and height. Their steepness is small, and they are more predictable than the sea waves. They are now called *swell*, and they can propagate for very long distances across a whole ocean basin without losing much of their energy, until they reach the coast and dissipate. The characteristics of the swell are accurately described by linear surface gravity wave theory.

Surface gravity waves are freely propagating oscillations that have as upper boundary the atmosphere and as lower boundary the sea bottom. While in deep water the bottom has little or no effect, as the waves approach shore, they start to “feel the bottom.” The presence of the seafloor affects the propagation of waves (shoaling and refraction) and causes friction that dissipates wave energy. The decrease in wave group speed from deep to shallow water causes an effect known as *shoaling*: the front of the advancing wave is slowed down, and the accumulation of wave momentum causes an increase in the wave height. This is particularly dramatic in the case of the destructive waves known as Tsunamis.

In addition to causing a change in amplitude due to shoaling, the dependence of the wave speed on the water depth also causes a change in the propagation direction of the waves known as *refraction* - in a similar way as the sound or light rays are bent as they pass through a medium where the propagation speed changes. Refraction is responsible for the bending of the wave fronts towards the shallower waters, and for the observed fact that waves arrive almost perpendicular to the coastline. A direct effect of refraction on the

wave field is that it can cause convergence or divergence of wave energy in areas with irregular bathymetry (convergence over shoals and divergence over trenches).

As the waves continue their approach to the shore, when the ratio between the wave amplitude and the depth exceeds a critical value, *depth-induced breaking* occurs. The area across which waves break is known as the surf zone, and it is where the remainder of the energy that was transmitted to the waves by the wind is lost.

2. Bottom Friction

The wave dissipation mechanism that is expected to be dominant in shallow water outside the surf zone is bottom friction. As waves travel, they induce pressure variations over the water column as well as orbital motions of water particles. The diameter of these orbits is greater at the surface and decreases down with depth. In deep water, the wave-induced water particle motion does not reach the sea bottom. In intermediate water, i.e., where the water depth is less than one-half of the wavelength, however, the water particle orbits extend down to the bottom. This leads to a direct interaction between the surface waves and the sea floor. Different mechanisms of wave-bottom interactions can be classified as: “scattering on bottom irregularities, motion of a soft bottom, percolation into a porous bottom, and friction in the turbulent boundary layer” (Komen et al., 1994, p. 156). Of these processes, the only one that is not a direct dissipative mechanism is scattering by the bottom, since it implies a redistribution of energy.

Motion of a soft bottom refers to the elasticity of the bottom that is excited by the variations of pressure due to the overlaying wave field. Sandy sea beds have some elasticity, but their movements are of small amplitude and are normally in phase with the wave-induced pressure field, so the effect on the wave field is not significant. Muddy bottoms, however, can absorb more energy from the waves (Gade 1958; Dalrymple and Liu, 1978; Trainor, 2009).

Percolation into a porous bottom induced by wave-induced pressure exerted on the sea floor can cause wave energy dissipation. The water inside the porous sediment will move with the variations in pressure. The movement of the water inside the sediment may not be in phase with the wave pressure field above it, causing a loss of energy.

Flow friction over the bottom creates turbulence in the boundary layer that dampens the wave orbital motion and its surface signature. Between the processes of percolation and bottom friction, whether one is dominant over the other depends on the type of bottom sediment, and on the bottom roughness. Lowe (2005) showed that coral reefs can dissipate wave energy by friction in a magnitude comparable to wave breaking. Over sandy bottoms, the size of sand grains is important. Coarse sand enhances percolation, while fine sand is favorable for friction. The presence of sand ripples, especially wave-induced vortex ripples with steep crests, greatly enhances bottom friction. On continental shelves sand ripples are ubiquitous (e.g., Traykovski et al., 1999; Ardhuin et al., 2002), and bottom friction is believed to be a dominant source of wave decay outside the surf zone (Young and Gorman, 1995; Herbers et al., 2000; Ardhuin et al., 2003).

A rigorous incorporation of bottom friction in wave prediction models is not feasible because of the difficulty to resolve turbulent flows down to the roughness scale of individual sand grains. As is the case for most of the other wave energy dissipation mechanisms, numerical wave prediction models rely on semi-empirical parameterizations of these processes obtained from field or laboratory experiments. In order to evaluate the wave energy dissipation due to bottom friction the product of two quantities is normally used, the velocity of the water particles near the bottom, and the shear stress immediately above the boundary layer. The velocity of the particles can be obtained easily from linear wave theory. The shear stress computation is more problematic, and here is where parameterizations are needed. Two principal types of models have been

developed to parameterize the shear stress (see Holthuijsen 2007 for a review): the drag law models, (e.g., Collins 1972), and the eddy-viscosity models, (e.g., Madsen et al., 1988).

The drag law models represent the shear stress over the bottom in a similar way as the wind shear over the sea surface is estimated, that is, by using a quadratic law with a drag coefficient (in this case bottom friction coefficient), which has to be determined empirically.

In the eddy-viscosity models, the parameterization of the shear stress is based on parameters of the sea bottom, such as the bottom roughness. For sandy bottoms, the roughness is controlled by the size of the sand grains.

These two types of bottom friction models can be formulated in the same form but with different estimates for the bottom friction coefficient. Between the two types, the eddy-viscosity models have a better physical foundation, but both approaches rely on semi-empirical coefficients that vary with flow conditions and seafloor morphology, and thus are difficult to specify.

Hasselmann et al. (1973) further simplified the parameterization of bottom friction based on results of JONSWAP (JOint North Sea Wave Analysis Project). Instead of a quadratic drag law, this approach uses a linear dependence on flow velocity with a constant coefficient. This is loosely based on the notion that increased forcing conditions often cause a reduction in drag coefficient. Despite its simplicity, this parameterization gives reasonable results over sandy bottoms (Young and Gorman, 1995).

Formulations for the mentioned bottom friction models will be discussed in more detail in Chapter IV, for some of them are implemented in the SWAN model, and will be used in the different model runs presented in this thesis.

C. PREVIOUS EXPERIMENTS ON WAVE TRANSFORMATION OVER CONTINENTAL SHELVES

From the numerous experiments on wave transformation found in the literature, three are considered to be relevant to the objective of this thesis, because they share a similar objective, i.e., the study of wave dissipation by bottom processes, as well as a similar methodology. All were carried out on continental shelves, and all used wave prediction models to isolate energy source/sink terms with the purpose of identifying those most dominant. The need to use wave models for these studies was pointed out by Komen et al. (1994), who concluded that up to then, observational knowledge of wave dissipation by interaction with the sea bottom was scarce. They attributed this absence of information to the lack of understanding of the different bottom processes, which makes it difficult to evaluate their contribution to wave decay observations. In order to obtain a good quantitative analysis, it is important to isolate the individual energy source/sink mechanisms in the data.

The first comprehensive experiment that yielded quantitative estimates of swell decay by bottom friction was carried out in the Great Australian Bight (Young and Gorman, 1995). Swell arriving from the Southern Ocean was monitored as it propagated across the continental shelf off the south coast of Australia. The width of the experiment area was about 250 km, and wave-measuring instruments were deployed from depths of 1200 meters up to 20 meters. Strong swell attenuation was observed throughout the experiment. The third-generation ocean wave prediction model WAM (WAve prediction Model) was used to account for processes such as refraction, shoaling, nonlinear interactions and whitecapping.

One important conclusion of this study was that the quadratic bottom friction parameterization gave better results if the bottom friction coefficient was not set to be constant, as it had been considered in the different models available at that time, but variable and inversely dependent on the particle velocity near the bottom. This result confirmed the representation of bottom friction coefficients in

the eddy-viscosity models, which also showed that dependence, as well as in the empirically estimated JONSWAP variable linear bottom friction formulation (Hasselmann et al., 1973), which relied also on the inverse dependence of the coefficient on the particle velocity near the bottom.

A few years later, in 1999, an experiment called SHOWEX (SHOaling Waves Experiment) was carried out on the North Carolina continental shelf (Ardhuin et al., 2003). In this experiment, an extensive array of wave- measuring instruments was deployed across a continental shelf width of about 100 km, in depths that ranged from 300 to 8 meters. During the experiment, several hurricanes passed through the area; therefore, extreme swell events could be monitored. The spectral wave prediction model CREST (Ardhuin et al., 2001) was used as a parameterization tuning tool. Strong attenuation of large swells was observed (typical height reductions were of a factor of two). Dissipation of up to 93% of the incident wave energy flux was recorded across the broadest part of the shelf. This decay occurred under very weak wind conditions, inferring that bottom processes were responsible for the wave dissipation. Furthermore, as might be expected, the swell dissipation was observed to be weaker where the shelf was narrower and in deep water. In contrast to the strong decay of hurricane swells, small swells, i.e., wave height less than one meter, were only weakly attenuated.

Recently, in 2008, an experiment over a muddy sea bed, MUDEX, was carried out on the Louisiana continental shelf (Trainor, 2009). Wave-measuring instruments were deployed in depths ranging from 13 to 4 meters covering an area of 40 by 25 km. The SWAN (Simulating Waves Nearshore) spectral wave prediction model was used to test its performance in a muddy environment, for which no specific parameterizations of bottom friction are available. The SWAN model will also be used in this thesis. The most relevant result of the MUDEX experiment is that the default SWAN parameterization of bottom friction (Hasselmann et al., 1973) performed quite well against the observations for low frequency waves, suggesting that swell decay may not be affected much by the

bottom elasticity. For higher frequency wind seas, however, the model did not perform well. These higher frequency waves were generated by local wind events that may cause suspension of mud over the entire water column, which in turn dissipates the wave energy in a different way than the friction at the bottom. Apart from the model performance results, observations showed that in the areas where the mud concentration at the bottom was the highest the largest wave attenuation occurred. The increased viscosity of the water column induced by mud suspension was suggested to be the cause of that strong decay.

The three earlier experiments discussed here have opened new avenues for optimizing the performance of spectral coastal wave models, in particular with respect to bottom friction effects. This thesis further contributes to this task by analyzing a new data set of wave measurements, and testing the observations against the results obtained from the SWAN model. The main difference between this experiment and the previous three is that the spatial domain across the continental shelf is much smaller since the deployed array spans only about five kilometers across the inner continental shelf. Thus, this thesis will focus in more detail on the nearshore environment to evaluate the effect of bottom friction and test the model performance. A description of the experiment, the field site, and the instruments used for wave data collection is given in the following chapter.

II. FIELD SITE AND DATA COLLECTION

The Martha's Vineyard Experiment, henceforth referred to in this thesis as MV2007, was part of a series of experiments funded by the Office of Naval Research that were carried out with the goal of better understanding the surface wave processes on continental shelves and beaches. Although the main objective of MV2007 was the study of seafloor ripples excited by the orbital motion of ocean surface waves, the measured wave field will be exploited in this thesis to analyze the wave evolution. What follows is a description of the experiment and of the various instruments deployed to measure waves.

A. DESCRIPTION OF THE EXPERIMENT

An extensive array of wave-measuring instruments was deployed in the fall of 2007 on the inner continental shelf off the southern coast of the island of Martha's Vineyard (Massachusetts). The continental shelf of that part of the U.S. East Coast extends about 180 km offshore (Figure 1). In contrast to the previous SHOWEX experiment (Ardhuin et al., 2003) which covered the entire continental shelf of North Carolina, the MV2007 array of instruments was concentrated within six kilometers from shore, in depths ranging from 24 to 10 meters (Figure 2), to measure in detail the wave evolution across the sandy inner shelf.

The southern coast of Martha's Vineyard receives swell generally from the South, generated by persistent strong winds associated with the Bermuda High. The array of instruments was oriented in an almost N-S direction, in order to match as closely as possible the mean swell direction. During the experiment, the offshore buoy DW1 recorded significant wave heights (Hs) that ranged from 0.2 to 3 meters, with dominant wave periods of 4 to 17 seconds (mean period 7.5 s), and the wave direction at the peak frequency fluctuated from the East (87º) to the West-South-West (250º) with a mean direction from the South (184º) (Figure 3).

An important aspect of the location of the instruments is that all of them were deployed outside the surf zone. Depth-induced wave breaking is generally believed to occur when the threshold parameter $\gamma = \frac{H}{h}$, a ratio between the wave height (*H*) and the water depth (*h*), exceeds a value of about 0.4 to 0.8 (Battjes and Janssen, 1978; Thornton and Guza, 1983; Battjes and Stive, 1985). This implies that at the shallowest sites, where the water depth is of the order of 10 meters, the wave height should be of the order of 4 to 8 meters in order for depth-induced breaking to occur. Such large wave heights were rarely observed during the experiment, so the instruments are assumed to have been operating outside the surf zone.

A brief description of the different types of wave-measuring instruments employed is presented below. The data analysis procedures are described in the following chapter.

B. WAVE-MEASURING INSTRUMENTS

The sensor locations are shown in Figure 1 (bottom panel). Two Datawell Directional Waverider buoys (DW) were deployed along the deeper part of the transect in depths of 24 and 21 meters. In the middle of the transect, in depths from 15 to 18 meters, a coherent array of eight bottom pressure transducers (PA) were positioned. Finally, six shallow water pressure-velocity (PV) tripods were deployed on the shallowest part of the transect, in depths from 10 to 13 meters**.**

1. Bottom Pressure Sensors (PA)

These instruments were mounted on tripods and lowered to the bottom (Figure 4). They measure wave-induced near-bottom pressure fluctuations. Pressure data were recorded continuously at a frequency of 2 Hz (a sample every 0.5 seconds). Time series of the measured pressure are available from all the PA sensors during almost the entire period of the experiment, except from PA5, which was operational only during the first ten days.

2. Bottom Pressure and Velocity Sensors (PV)

These instruments were also mounted on tripods and positioned at the bottom (Figure 5). The instrument package included a Nortek Vector acoustic Doppler velocimeter that measures velocity fluctuations with respect to three axes at a fixed point above the instrument, and a Nortek Aquadopp acoustic Doppler profiler that measures velocity profiles and served as a redundant wave sensor. Both the Vector and Aquadopp instruments also include a pressure gauge.

Data from the PV sensors were recorded in two separate sets, for in the middle of the experiment the tripods were turned around and redeployed a few days later. The Vector pressure and velocity data (used in this thesis) were collected in bursts of 68.27 minutes every four hours, at a sampling frequency of 2 Hz. Since the velocity was measured with respect to a compass heading, magnetic declination corrections were applied to obtain velocities with respect to the true north.

3. Waverider Buoys (DW)

The offshore wave measurements were obtained with two surface-following Datawell Directional Waverider buoys (Figure 6), which were moored at the bottom. Displacements along three orthogonal axes are measured with a three-component accelerometer package, tilt sensor, and compass. The horizontal displacements are recorded with respect to the magnetic north heading of the compass. Displacements are sampled continuously at a frequency of 1.28 Hz (sampling interval 0.78 seconds) in blocks of 30 minutes. A magnetic declination correction was applied to reference the horizontal displacements to true north.

The most offshore waverider buoy, DW2, was not operational during part of the experiment (Figure 7). This failure limited its use as the sensor that was to

provide the spectral wave information at the boundary of the numerical model domain. Instead, DW1 was used for this purpose since it was operational during the entire experiment.

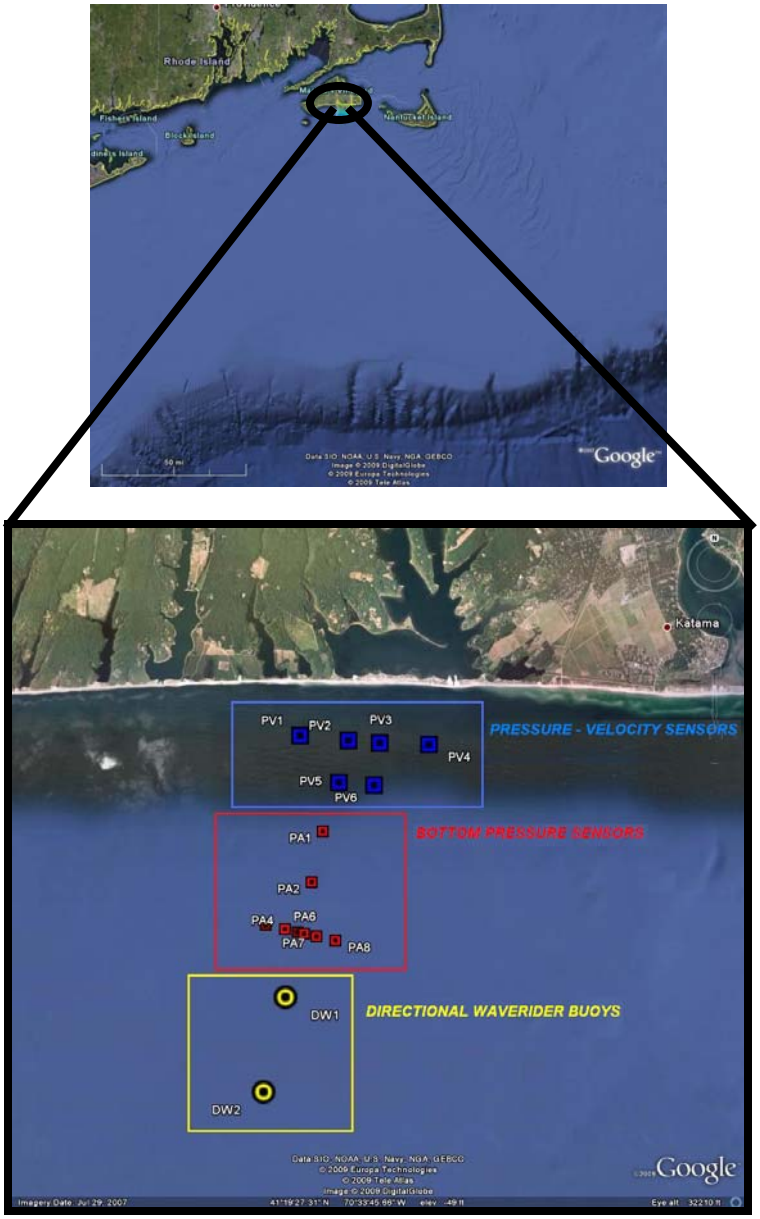

Figure 1. Overview of the experiment site near the island of Martha's Vineyard and surrounding continental shelf. The width of the continental shelf (top panel) (the edge is marked by the sharp transition region with canyons near the bottom of the graph) is about 180 km. The MV2007 experiment was carried out off the southern coast of the island. The wave-measuring array of instruments is shown in the bottom panel. The array spanned about 5 km across the inner continental shelf, outside of the surf zone (From ©Google (2009)).

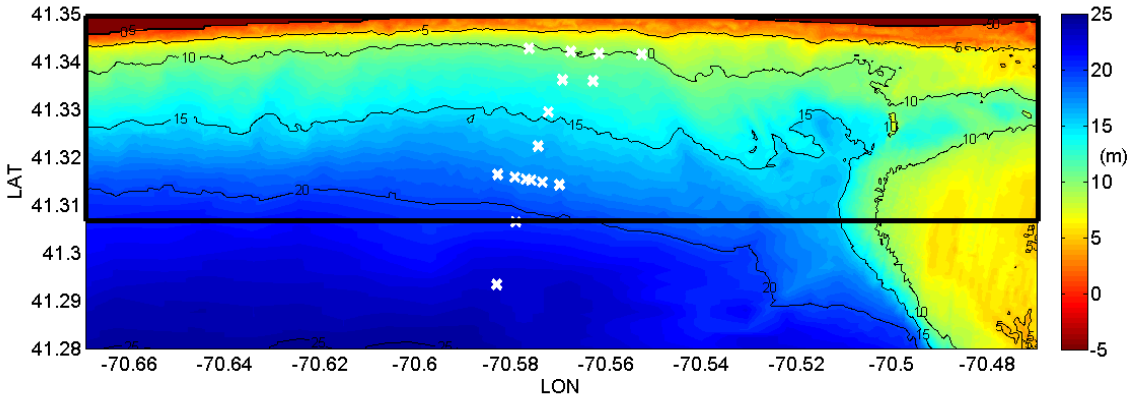

Figure 2. The MV2007 experiment field site on the inner continental shelf south of the island of Martha's Vineyard. Depth contours every 5 meters are shown. The 16 wave-measuring instruments were located in depths ranging from 24 to 10 meters. Land is shown in dark red. The overlaying box (approx. 16.7 km x 4.8 km) indicates the boundaries of the computational grid used for the SWAN model runs. High-resolution bathymetry data was obtained from the National Ocean Service Hydrographic Data Base (NOSHDB).

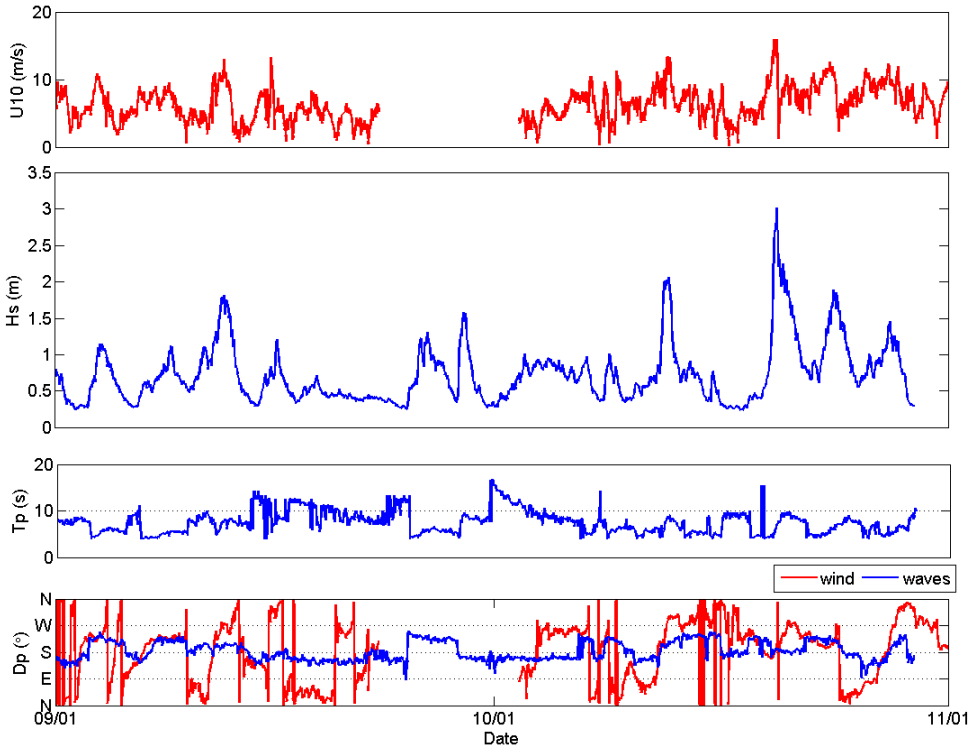

Figure 3. Time series of wind (red curves) and wave (blue curves) data. Panels from top to bottom: wind speed at 10 meters elevation (U_{10}), significant wave height (*Hs*), wave peak period (*Tp*), wave mean direction at the peak period (*Dp*) and wind direction (from). Measured winds at an elevation of 18.4 m above mean sea level were corrected to 10 m elevation using a logarithmic wind profile with a roughness length determined by Charnock's (1955) relation (coefficient value 0.0144).

Figure 4. One of the eight bottom pressure sensors (PA) mounted on a tripod deployed in the MV2007 experiment.

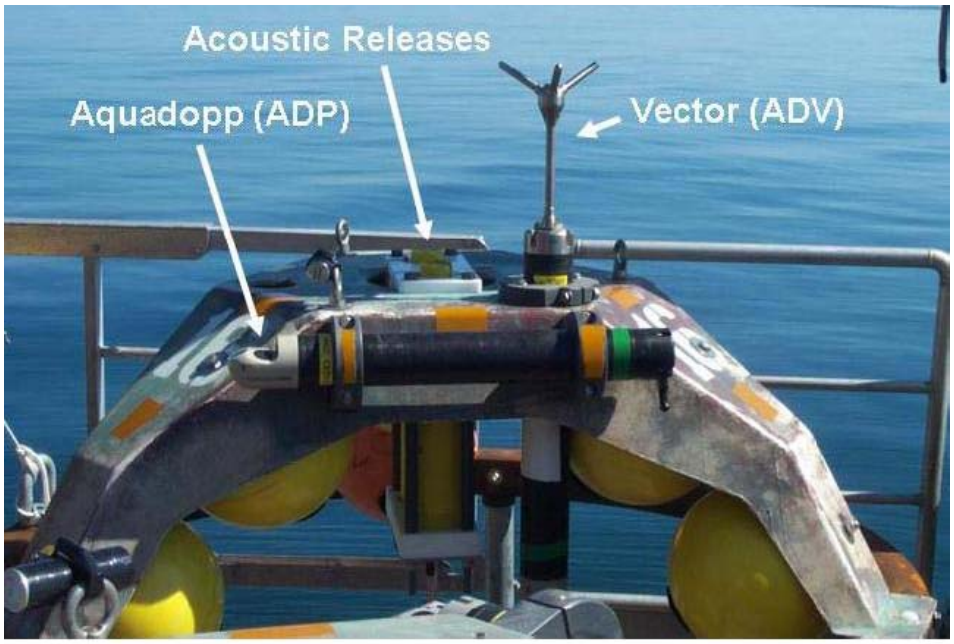

Figure 5. One of the six shallow water Pressure – Velocity tripods (PV) deployed in MV2007. Pressure and velocity were measured by both the Vector and Aquadopp instruments to have data redundancy in case an instrument failed (see Trainor, 2009, for further details about the equipment).

Figure 6. One of the two Datawell Waverider buoys deployed in the MV2007 experiment.

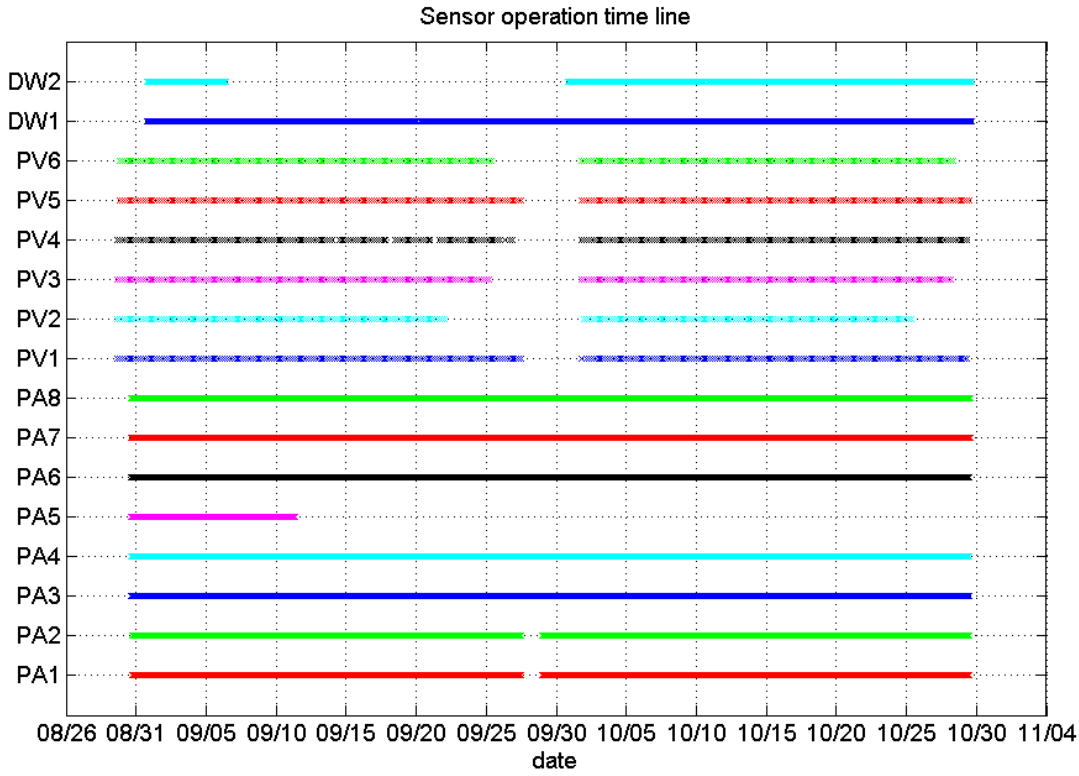

Figure 7. Table showing the times when the 16 wave-measuring instruments were operational during the MV2007 experiment. The shallower of the two directional waverider buoys (DW1) was selected to provide the boundary conditions for the SWAN model runs, since DW2 was not operational during the whole period.

THIS PAGE INTENTIONALLY LEFT BLANK

III. DATA ANALYSIS

In this chapter a description of the analysis of the recorded wave data is given. The goal of this analysis is to obtain certain bulk parameters of the waves, such as significant wave height (*Hs*), peak period (*Tp*), and mean propagation direction at the peak period (*Dp*), as well as frequency spectra and directional spectra. These estimates will allow quantitative comparisons with the SWAN model output wave information.

In addition to wave data, wind data were recorded by a sonic anemometer located on the Woods Hole Air-Sea Interaction Tower (ASIT), a meteorological tower in 15 meters depth in the middle of the experiment site (operated by the Woods Hole Oceanographic Institution). The time series (Figure 3; courtesy of Drs. John Trowbridge and Janet Fredericks) show that the wind blew from all directions during the experiment, with a mean direction from the South (180º). The wind speed ranged from almost no wind to 16 m/s, with a mean speed of 6.5 m/s. There was an 8-day period in the middle of the experiment when no wind data were recorded.

Wave data were recorded at the 16 array sites from August 31 to October 30, 2007. Most of the instruments were operational during the entire period (Figure 7), with the exception of a few days in late September when instruments were serviced and data retrieved. Partial data sets were retrieved at two sites (DW2 and PA5) owing to instrument failures.

A. SPECTRAL ANALYSIS

In order to estimate the various bulk wave parameters, first the distribution of wave energy (or more specifically the distribution of the variance of the surface elevation) across the frequency range of 0.05 to 0.25 Hz was computed using the MATLAB Signal Processing Toolbox. Frequencies below 0.05 Hz were excluded because the “infra-gravity motions” at these frequencies are relatively weak and

require a different analysis approach that is outside the scope of this thesis. Frequencies higher than 0.25 Hz were also excluded because these short wavelength waves are attenuated at the seafloor where most of the instruments were located. From the surface elevation spectrum, the significant wave height (*Hs*) and the peak period (*Tp*) can be estimated as outlined below. To obtain directional information, a cross-spectral analysis of the measured time series was performed to estimate the mean wave direction at each frequency and its value at the peak period (*Dp*). The convention used to indicate directions was the nautical convention, that is, where the waves "arrived from."

1. Surface Elevation Spectra

The PA and PV sensors recorded times series of sub-surface pressure that were converted to equivalent heights of the water column (by using the hydrostatic equation $p = \rho g h$, where ρ is the water density, g is the acceleration of gravity, and *h* is the height of the water column) ; linear wave theory can be applied to extract the surface elevation spectrum from the pressure spectrum, which can be obtained from the pressure time series. The relation between the time series of the demeaned dynamic pressure, i.e., that induced by the wave, (p) (expressed in units of water column height) and the time series of the surface elevation (η) is given by:

$$\eta(t) = p(t)\frac{\cosh(kD)}{\cosh(kd)} \qquad (1)$$

where *k* is the wave number, *D* is the water depth, and *d* is the elevation of the pressure sensor above the sea bottom. The wave number at a given frequency (f) can be obtained from the dispersion relation

$$\omega^2 = (2\pi f)^2 = gk\tan kD \qquad (2)$$

Relation (1) constitutes a linear system constant in time, in which the pressure values are multiplied by a transfer or response function

$H(f) = \frac{\cosh(k(f)D)}{\cosh(k(f)d)}$. The corresponding response spectrum of the surface elevation $E_\eta(f)$ is related to the pressure spectrum $E_p(f)$ by

$$E_\eta(f) = E_p(f)\left|H(f)\right|^2 \quad (3)$$

In the case of the DW buoys, since they measure vertical displacements following the surface, the surface elevation spectrum can be computed directly from the recorded time series of those displacements.

Once the surface elevation spectrum is calculated, the significant wave height *(Hs)*, which is defined as the mean value of the highest one-third of wave heights, can be estimated by means of the following widely used formula:

$$Hs \approx 4\sqrt{\int_{0.05}^{0.25} E_\eta(f)df} \quad (4)$$

where in this case the integral is computed between the two frequency limits.

The peak frequency and the corresponding peak period *(Tp)* can be obtained by identifying from the spectrum the frequency with maximum energy.

2. Directional Spectra

Wave direction information can be estimated from both the DW and PV sensors. A mean wave propagation direction as a function of frequency $\theta_{mean}(f)$ can be defined in terms of the first Fourier moments, a_1 and b_1, of the normalized directional distribution of wave energy $S(\theta; f) = \frac{E(f,\theta)}{E(f)}$ (Longuet-Higgins et al., 1963):

$$\theta_{mean}(f) = \tan^{-1}\left(\frac{b_1(f)}{a_1(f)}\right) \quad (5)$$

where

$$a_1(f) = \int_{-\pi}^{\pi} S(\theta; f)\cos\theta d\theta \quad (6)$$

$$b_1(f) = \int_{-\pi}^{\pi} S(\theta; f)\sin\theta d\theta \quad (7)$$

These two directional moments can be estimated directly from the cross-spectra of the measured quantities, i.e., *p, u, v* measurements in case of the PV sensors, and *x, y, z* displacements in case of the DW sensors. For the PV sensors, the normalized co-spectra (C) of pressure *p* and the velocity components *u, v*, is used (e.g. Herbers et al., 1999 and references therein):

$$a_1(f) = \frac{C_{pu}(f)}{\left\{C_{pp}(f)\left[C_{uu}(f) + C_{vv}(f)\right]\right\}^{1/2}} \quad (8)$$

$$b_1(f) = \frac{C_{pv}(f)}{\left\{C_{pp}(f)\left[C_{uu}(f) + C_{vv}(f)\right]\right\}^{1/2}} \quad (9)$$

For the DW sensors, the directional moments can be estimated from the normalized quadrature (Q) spectra of the vertical (*z*) and horizontal (*x, y*) buoy displacements (equivalently heave, east-west horizontal translation, and north-south horizontal translation) (Longuet-Higgins, 1963):

$$a_1(f) = \frac{Q_{zx}(f)}{\left\{C_{zz}(f)\left[C_{xx}(f) + C_{yy}(f)\right]\right\}^{1/2}} \quad (10)$$

$$b_1(f) = \frac{Q_{zy}(f)}{\left\{C_{zz}(f)\left[C_{xx}(f) + C_{yy}(f)\right]\right\}^{1/2}} \quad (11)$$

From the spectrum of estimated mean directions $\theta_{mean}(f)$ along with the surface elevation spectrum $E(f)$, the mean direction at the peak frequency (*Dp*) can be identified.

This spectrum of mean directions is not a 2-D frequency-direction spectrum, since it only describes the mean direction at every frequency. To

compute a 2-D frequency-direction spectrum $E(f,\theta)$, needed as input for the boundary condition information for the model SWAN, the Maximum Entropy Method (MEM) (Lygre and Krogstad, 1963) was applied to the *x, y, z* displacements measured by buoy DW1.

3. Data Processing Details

The PA sensors recorded time series of pressure nearly continuously at a sampling frequency of 2 Hz. The PV sensors recorded time series of pressure and velocity also at a sampling frequency of 2 Hz, but in bursts of 68.27 minutes every four hours. On the other hand, the DW sensors recorded time series of *x, y, z* displacements continuously at a sampling frequency of 1.28 Hz.

In order to compare the observed wave statistics and spectra at all instrument sites for the same time intervals and using the same processing scheme, bursts of 68.27 minutes were extracted from each instrument every four hours, and the DW sensor data were interpolated in time to obtain an equivalent record with a sampling frequency of 2 Hz, instead of 1.28 Hz.

The record length of 68.27 minutes contains 8192 samples that were divided into segments of 256 points with 50% overlap, yielding spectra and cross-spectra estimates with 64 degrees of freedom.

B. OBSERVED WAVE STATISTICS

From 68-minute bursts, the surface elevation spectra at the PA, PV, and DW sensor sites, and the mean direction spectra at the PV and DW sensor sites were computed. From these spectra, bulk parameters of significant wave height (*Hs*), peak period (*Tp*), and mean direction at the peak period (*Dp*) were estimated. Time series of these bulk parameters helped to identify events with a range of wave conditions for further analysis and SWAN model hindcasts. As mentioned before, the offshore DW2 sensor was not used since it was not operational during the whole experiment. Observed variations in wave statistics between DW2 and DW1 were generally small.

Examining the bulk parameters time series (Figures 8 and 9) a general decay of the wave height Hs from offshore to onshore can be clearly seen, mostly during the more energetic events, which in some cases is of the order of 15–20% of the incident wave height. A primary goal of this thesis is to identify the processes that cause this decay. The period *Tp* does not vary much from offshore to onshore, which was expected considering the relatively short transect. The longest periods were observed in low energy conditions, indicative of remotely generated swell. However, some of the energetic wave events, i.e., Hs peaks in Figures 8 and 9, were observed to have wave periods of more than 8 seconds.

The observed mean direction at the peak period (*Dp*) was also relatively uniform across the array, bending towards 180º (normal incidence) at the shallowest site PV2, as expected from refraction theory.

C. CASE STUDIES

From the time series of the bulk wave parameters at three sites in the central transect of the array, offshore (DW1), middle (PA2) and onshore (PV2), a total of six case studies were selected (Figures 8 and 9), one in the month of September and the other five in the month of October. The case studies each use a single burst with a duration of 68.27 minutes, that is long compared with the time it takes waves to traverse the 5-km long transect (about 10 minutes for 10-second period waves). The criteria used to select them were based on the variation in *Hs* observed across the transect and the values of the bulk parameters observed at the DW1 site. The selected cases span a range of wave heights, periods, and directions in order to cover diverse wave fields. Wave fields with very large oblique propagation directions, that is, those with a *Dp* greater than 225º or smaller than 135º at the offshore buoy, were discarded because they would be affected greatly by refraction and thus other processes would be difficult to identify. Wave fields with long period *Tp* were preferred, because they "feel the bottom" more than those with shorter periods. Of particular interest were

energetic wave conditions when strong damping might be expected. Case 5 was the most energetic event of the experiment with an offshore significant wave height of 2.6 meters. Two less energetic events, cases 2 and 3 with *Hs* less than one meter were selected, with moderate oblique incidence angles from opposite quadrants to investigate the effects of refraction on the wave transformation.

Figure 10 shows the energy density spectrum and the mean direction spectrum at the DW1 site for the six case studies. The legend of the figure shows the bulk parameters corresponding to each of them. Most of the cases are dominated by swells with periods over 8 seconds. Case 3 shows more energy in shorter period waves, but since the wind speed recorded at that time was very small (~ 1 m/s), these waves were in fact shorter period swell from a nearby generation source. Winds with a West to South-West component and speeds just above 8 m/s were recorded in cases 4, 5, and 6, which are the most energetic. The spectra of these cases are broad, dominated by swells of periods over 8 seconds with active wind-sea components at higher frequencies.

The mean direction spectra of the six case studies show a wide range of direction, especially at the higher frequencies. In some cases (e.g., 1 and 2) the directions of low frequency swells and higher frequency wind waves differ by as much as 60 degrees.

The wave field parameters observed at the other sensor sites will be discussed in Chapter V, along with the predicted values by SWAN.

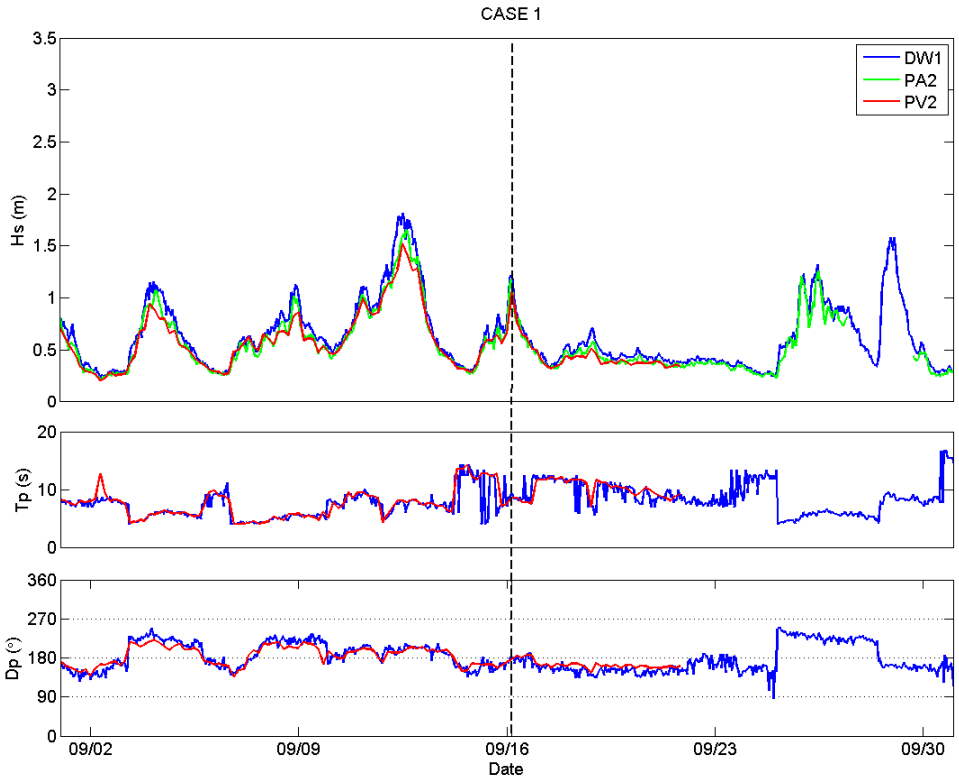

Figure 8. Time series of the bulk parameters significant wave height *Hs* (top panel), peak period *Tp* (central panel), and mean direction (from) at the peak period (*Dp*) (bottom panel), at sites of the central transect sensors DW1, PA2, and PV2, during the month of September. The time corresponding to Case 1 is indicated with a dashed line.

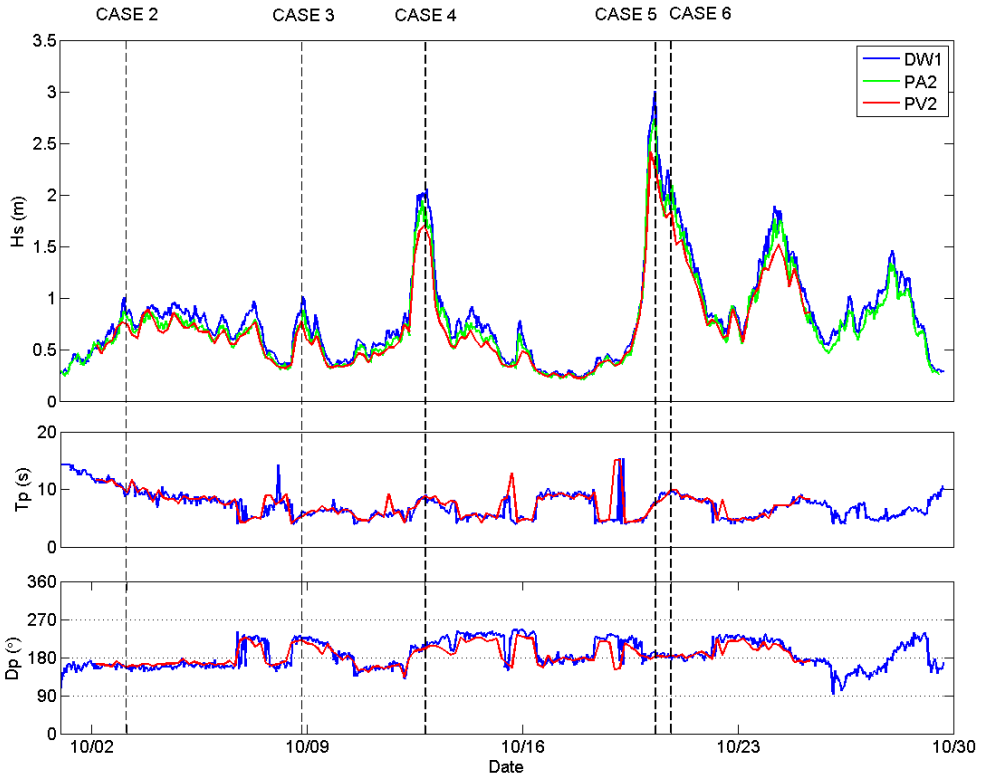

Figure 9. Same as figure 8, but for the month of October. The times for Cases 2 to 6 are shown.

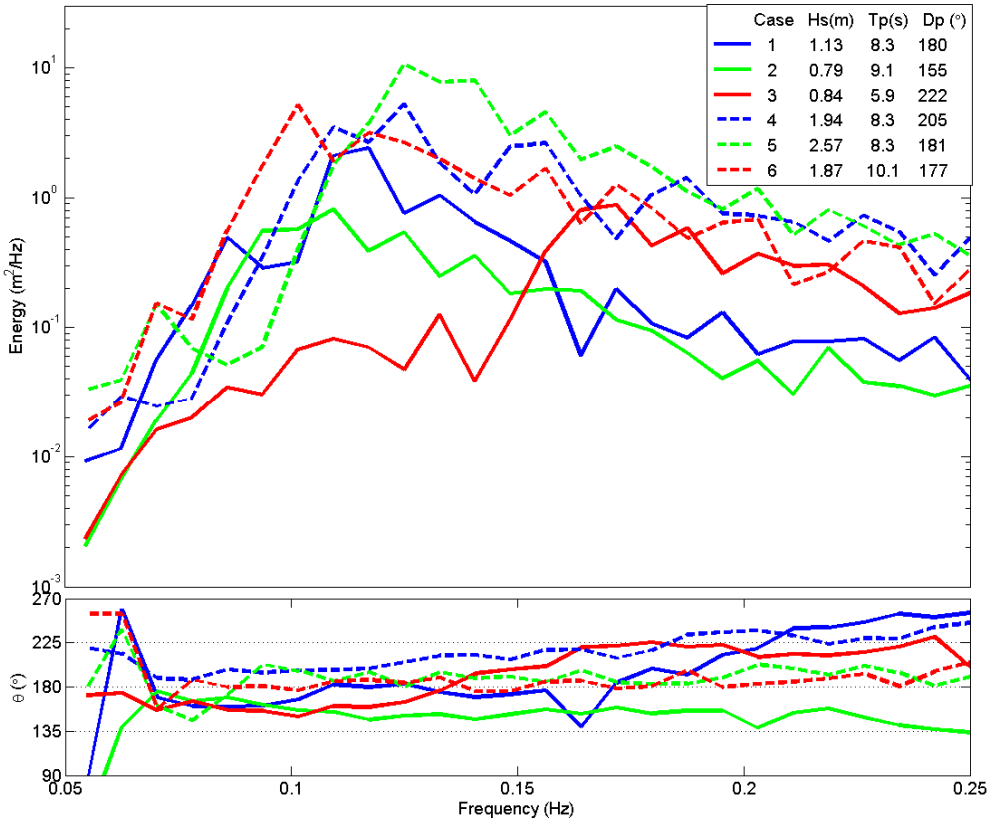

Figure 10. Energy density spectrum (top panel) and mean direction spectrum (bottom panel) at the offshore site DW1 for the six case studies. Bulk wave parameter values are listed in the legend.

IV. THE SWAN MODEL

A. DESCRIPTION OF THE MODEL

The numerical wave prediction model SWAN (Simulating WAves Nearshore) was developed by the Delft University of Technology (The Netherlands), (Booij et al., 1999). It is a third generation wave prediction model in which "the spectrum is free to develop without any shape imposed a priori" (Holthuijsen, 2007, p. 196). The model is designed to be employed in coastal areas (in shallow waters), and is widely used by the military community as well as scientists and engineers. In order to efficiently run the model in littoral areas, where high spatial resolution is required to resolve the coastline and bathymetry effects, SWAN uses implicit propagation schemes, that are stable for arbitrary time steps, i.e., the Courant criterion is met (e.g., Kantha and Clayson, 2000).

If no currents are taken into account, as in the present study, the SWAN computations are based on the Eulerian energy balance equation, which is generally expressed in spherical coordinates as (e.g. The WAMDI Group, 1988):

$$\frac{\partial E(f,\theta;\lambda,\varphi)}{\partial t}+\frac{\partial c_{g,\lambda}E(f,\theta;\lambda,\varphi)}{\partial \lambda}+\frac{1}{\cos\varphi}\frac{\partial c_{g,\varphi}E(f,\theta;\lambda,\varphi)}{\partial \varphi}+ \\ +\frac{\partial c_{g,\theta}E(f,\theta;\lambda,\varphi)}{\partial \theta}=S(f,\theta;\lambda,\varphi) \qquad (12)$$

where $E(f,\theta;\lambda,\varphi)$ is the 2-D energy density spectrum (depending on frequency and propagation direction) at a fixed point of longitude λ and latitude φ, and c_g is the wave group speed. The first term on the left hand side is the local variation in time of E, the following two terms represent the advection of E by the group velocity c_g in longitude and latitude (i.e., the divergence of the energy flux ($c_g E$) in longitude and latitude). Since c_g in shallow water varies with depth ($c_g=\sqrt{gH}$), shoaling is accounted for in these two terms. The following term is the variation

of energy density due to depth-induced refraction. The right hand side of the equation represents the local energy sources and sinks. This term, known as the source term, is expressed as:

$$S = S_{in} + S_{nl} + S_{diss} \tag{13}$$

where S_{in} represents generation by wind, S_{nl} nonlinear wave-wave interactions, and S_{diss} dissipation. Exact formulations of the components of the source term are not feasible because the processes are not well understood (S_{in}, S_{diss}), or the computational effort is prohibitively expensive (S_{nl}), and thus they need to be parameterized. A detailed description of the source term parameterizations can be found in Holthuijsen (2007). Of primary interest in this study is the dissipation source term that includes contributions due to whitecapping, depth-induced breaking, and bottom friction.

Several bottom friction parameterizations (see Chapter I, section A.2) are available in SWAN. They are all based on the same formula:

$$S_{diss,b}(f,\theta) = -C_b \left(\frac{2\pi f}{g \sinh(kD)} \right)^2 E(f,\theta) \tag{14}$$

where C_b is the bottom friction coefficient and *D* is the water depth. Three different formulations are implemented in SWAN: the drag law model formulation (Collins, 1972), the eddy viscosity model formulation (Madsen et al., 1988), and the empirical JONSWAP model formulation (Hasselmann et al., 1973). With respect to equation (14), the following applies for the different formulations:

- For the drag model, $C_b = C_{Collins}\, g u_{rms,b}$, with $C_{Collins} = 0.015$ and where $u_{rms,b}$ is the root-mean-square bottom orbital velocity, that is obtained from linear wave theory.

- For the eddy viscosity model, $C_b = C_{Madsen} g u_{rms,b}$, with $C_{Madsen} = \frac{f_w}{\sqrt{2}}$ where f_w is a non-dimensional friction factor that has different values depending on the (equivalent) bottom roughness length scale and the near bottom excursion amplitude.

- For the JONSWAP model, $C_b = C_{JONSWAP} = 0.038 m^2/s^3$ for swell conditions and $C_b = C_{JONSWAP} = 0.067 m^2/s^3$ for fully developed wind sea conditions in shallow water. In addition to these constant coefficients, a variable coefficient is also available that varies linearly between those two values depending on the frequency-dependent directional spreading (swell conditions are supposed to have the lowest directional spreading while wind sea conditions are assumed to have the highest).

If SWAN is implemented in stationary mode, as it is for this thesis, the first term of the left hand side of equation (12) can be removed. This approximation is valid in the case of waves that propagate through the model computational grid area in a short period of time relative to the time scale of variations in wave boundary conditions, wind, etc. A justification of the use of the stationary mode is given in the next section.

From the model runs, different wave parameters over the computational grid are computed. For this thesis the important ones are significant wave height (*Hs*) and mean direction at the peak period (*Dp*). Model output results will be compared with observations in the following chapter.

B. MODEL IMPLEMENTATION

SWAN Cycle III version 40.72AB was used in this thesis. Since SWAN is a freely available computer model, it was downloaded directly from the Delft University Web site (The SWAN team, 2009). The model has the advantage that output is created in files with the format used by MATLAB, which allows the use of its powerful computing and plotting capabilities to manage the results.

The model computational grid was set to be rectangular, and its geographic location can be seen in Figure 2, where it is overlaid on the available high-resolution bathymetry. It has the same lateral boundaries, 070º.67 W - 070º.47 W, and the same northern boundary, 41º.35 N, as the bathymetry grid. The southern boundary was set to coincide with the latitude of the DW1 site (41º.3065 N). The grid spacing was set to be the same as the bathymetry grid, that is, 0º.0002 (approx. 16.7 meters in longitude and 22.2 meters in latitude), which yielded 1001 grid points in longitude and 218 grid points in latitude (approx. 16.7 km x 4.8 km). The array of instruments lies almost in the middle of the longitudinal range of the computational grid, and despite the fact that the lateral boundaries were set quite far from the array relative to its cross-shore length, some effects near those boundaries are seen in some of the case studies, which will be discussed in the next chapter.

SWAN was run in stationary mode. The offshore depth of 21 meters implies a shallow water wave group speed of about 10 m/s. Thus the dominant waves propagate onshore across the computational grid in about 6–8 minutes while slower higher-frequency waves take about 10–20 minutes to cross the array. On these time scales, the wave field conditions at the boundary and the wind conditions usually do not change significantly, and so the assumption of stationary conditions is reasonable for this study.

The frequency limits for the model runs were set to be 0.05 Hz to 0.25 Hz, and the directional resolution was set at 5 degrees.

1. Boundary Conditions

The boundary conditions for the model runs, in the form of 2-D frequency-directional spectra, were set to match the observed spectrum at the buoy DW1 for each of the six selected case studies. This implies that SWAN considers a uniform wave field along the entire southern boundary. In the vicinity of the lateral boundaries the wave field that is generated by SWAN may not be realistic, because the lateral boundary causes a sheltering effect for waves that arrive at

oblique angles. The lateral boundaries need to be far enough from the area of interest so the lateral boundary shadowing effect does not reach the locations of model-data comparisons. The model domain size and location of the array in the computational grid area were carefully chosen to mitigate unwanted lateral boundary effects. Also, the array was located sufficiently far from the shoals off to the east, and thus their effect on the waves is not expected to reach the array. Nevertheless, there are some case studies where lateral boundary effects are present. This will be discussed in more detail in the following chapter.

2. Bottom Friction Parameterizations

SWAN was run for each of the case studies with several bottom friction parameterizations. Each case study was run in eight different modes, each one corresponding to a particular bottom friction setting. Table 1 shows these settings as well as the names given to identify the different SWAN modes. The “default” mode corresponds to the setting that SWAN uses by default when run with the friction source activated. The bottom coefficient used is the JONSWAP coefficient determined for fully developed wind sea conditions in shallow water. The “no friction” mode corresponds to runs with the friction “turned off.” Friction was also turned off in the “flat bottom” mode runs, where a bathymetry grid with a constant depth of 21 meters (the depth at the offshore DW1 site) was fed into the model. The purpose of using the “no friction” and the “flat bottom” runs was to isolate the contributions to the wave field decay due to refraction and bottom friction.

Modes “friction 2” to “friction 5” had the friction parameterization set to four different models (Table 1), and along with the “default” mode they were run to examine the performance of the different parameterizations. Finally, the mode “no sources” not only had the friction turned off, but all the other source terms (equation 13) were turned off as well, and the bottom was set to be flat (21-meter depth). With this configuration, the wave field at the southern boundary was free

to propagate across the computational domain, and any predicted energy variations may identify unwanted lateral boundary effects or other computational errors.

The results of these runs will be discussed in more detail in the next chapter, where they will also be compared to the observations, with the purpose of identifying the bottom processes that affect the wave transformation, and testing the performance of the model bottom friction parameterizations.

SWAN mode	FRICTION setting	REMARKS
DEFAULT	*JONSWAP coeff.: 0.067 m^2/s^3*	*For wind sea conditions*
FRICTION-2	*JONSWAP coeff.: 0.038 m^2/s^3*	*For swell conditions*
FRICTION-3	*JONSWAP coeff. Variable*	
FRICTION-4	*COLLINS coeff.: 0.015*	
FRICTION-5	*MADSEN scale(*): 0.05 m*	*(*) Equivalent roughness scale of the bottom*
NO FRICTION	*OFF*	
FLAT BOTTOM	*OFF*	*Constant depth: 21 meters*
NO SOURCES	*OFF*	*Constant depth: 21 meters All Sources turned off*

Table 1. SWAN model run configurations for each of the six case studies. The SWAN mode is the name given to the different configurations. All the friction parameterization settings available in SWAN are present. See text (Chapter IV, section A) for explanations of the bottom friction parameters.

V. WAVE TRANSFORMATION RESULTS

A. PROCESS IDENTIFICATION WITH SWAN

As discussed in the previous chapter, the SWAN model was run with different parameterization configurations with the purpose of isolating the processes that contribute to the decay of the wave field energy across the computational domain. The energy decay was quantified by the variation of significant wave height, a widely used parameter that is proportional to the square root of the local wave energy.

By comparing the “flat bottom” (with no friction) and the “no friction” model runs, the effects of shoaling and refraction on wave height evolution are isolated. With the “flat bottom” run all wave-bottom interaction processes are eliminated, and the remaining wave evolution is the result of other wave generation or dissipation processes. With the “no friction” run only bottom friction is eliminated, while shoaling and refraction effects are retained. Thus, from the comparison of these two model runs, the combined effect of shoaling and refraction can be estimated.

In order to quantify any other processes that may cause wave energy dissipation (e.g., wave breaking) or generation (wind input), SWAN was run with “no sources” over a flat bottom. Differences between this run and the “flat bottom” run would indicate the presence of any of those other sources or sinks.

For each of the six case studies, the results of the “flat bottom,” “no friction,” “default,” and “no sources” runs are compared in Figure 11. The variation of SWAN computed *Hs* versus latitude is shown across the central transect of the array of instruments (connecting the DW1 site with the PV2 site). The wave height predictions are normalized by the value at the DW1 site to quantify the decay.

1. Predicted Energy Dissipation

The first important result from the model inter-comparison in Figure 11, is that the predictions of the “no sources” and “flat bottom” runs are almost identical. This indicates that no other sources, apart from bottom friction, implemented in SWAN (equation 13) contribute significantly to the wave decay. This is not surprising as wind-wave generation effects are expected to be small over this relatively short distance. This result indicates that the wave evolution is dominated by bottom processes. In theory, the variation of *Hs* should vanish in the “no sources” run. The *Hs* variations are small indeed in cases 2, 5, and 6, but in the other cases some wave decay is observed in those runs, especially in Case 4 where the decay is of the same order as the effect caused by refraction. The cause of this numerical inaccuracy is likely a lateral boundary contamination effect associated with waves propagating into the computational grid at large oblique angles, which causes an artificial “shadow” at the lateral boundary. As evidence of this, in the bottom panel of Figure 11, the SWAN *Hs* output from the “no sources” run for Case 4 is shown. It can be seen that the shadowing effect of the western boundary affects the array site causing wave decay in the onshore direction.

The *Hs* variation from the “default” run was also included in the plots to quantify the decay predicted by the default bottom friction parameterization in SWAN. By comparing the *Hs* variation in the “default” run with that in the “no friction” run, it can be seen that as the waves advance across the central transect, bottom friction increasingly reduces the wave height, and this reduction is in all cases greater than that from the “no friction” run. The wave height decay across the array that would be due to bottom friction, if the SWAN parameterization is correct, is estimated to be of about 4–6% of the incident wave height.

2. The Effect of Refraction

Another important result is obtained from Figure 11 by comparing the predictions of the “flat bottom” and the “no friction” runs. The difference quantifies the effect of the energy conserving processes of shoaling and, more importantly, refraction on the wave evolution. In cases with obliquely incident waves, refraction causes a reduction of the wave height at the shallowest instrument of about 5–7% of the incident wave height. Whereas in most cases the wave height decays gradually towards the shore, in Case 2 the predicted wave heights show more variations. In this case, with waves arriving from the South-East, refraction induced by the irregular bathymetry (see Figure 2) in the eastern part of the domain is likely the cause of the Hs fluctuations generated by SWAN.

3. The Combined Effect of Refraction and Bottom Friction

The predicted combined effect of refraction and bottom friction is two-dimensional with *Hs* variations not only across the central transect, but over the entire computational area as can be clearly seen in Figures 12 and 13. These figures show for each case study the *Hs* field computed by SWAN in “default” mode. Overlaid on the *Hs* field are arrows showing the mean direction at the peak period (*Dp*) throughout the area. Figure 12 shows the three less energetic cases, each one with a different offshore wave direction. Figure 13 shows the three most energetic cases, with wave directions close to normal incidence.

In Case 1 and Case 6 waves are nearly normally incident. Whereas directions do not change much, wave heights are reduced, especially in Case 6, which is more energetic. In addition to the cross-shore decay, the model predictions also show alongshore variations in wave height that are most pronounced close to shore. These variations are caused by refraction over the irregular nearshore bathymetry (Figure 2).

Cases 3 and 4 have a similar South-Westerly swell arrival direction. Again the direction *Dp* remains nearly constant throughout the area except near the

eastern boundary where in Case 4 more variation of *Dp* is observed. Stronger dissipation can also be seen in the more energetic of the two cases, Case 4 (in areas outside the influence of the western boundary shadow). The two-dimensional refraction effects are less pronounced than in the normal incidence cases 1 and 6.

Case 3 shows the least variation in *Hs* and *Dp*. This is likely due to the fact that the incoming wave field had the shortest period, and thus it “felt the bottom” to a lesser degree.

Case 5 is the most energetic of all, with waves arriving at a slightly oblique (westerly) angle. Both dissipation and refraction effects contribute to the wave height variations with a similar pattern as in the other cases.

Finally, Case 2 is interesting because it has an easterly swell arrival angle resulting in more pronounced refraction effects to the east of the array.

4. Summary of Predicted Dominant Processes

The results from the model output information shown in Figures 11, 12, and 13 can be summarized as follows:

- No other sources, apart from bottom friction, implemented in SWAN appear to contribute significantly to the predicted wave decay.

- Refraction due to the irregular bottom topography causes variations in the incident wave height (Figure 14). Across the array central transect, decay on the order of 4–6% of the incident wave height is predicted. The default configuration of bottom friction active in SWAN shows that this process causes a wave decay of the order of 5–7% across the central transect. This makes the combined effect of bottom friction and refraction responsible for decay of 9–13% of *Hs* across the array.

- Throughout the rest of the computational domain, however, locally larger *Hs* decay is predicted, in some cases of the order of 20%. The wave decay across the inner shelf is seen to be larger in the cases where the wave field is

more energetic offshore and the wave period is longer, as well as in the areas where the bottom topography is more irregular. In these areas of irregular topography, there is also a larger variation in the mean direction of the waves.

Following this analysis of the numerically predicted wave evolution, a comparison with the observed wave evolution across the array of instruments will be given in the following section.

B. MODEL-DATA COMPARISON

Significant wave height observations for the six case studies are compared with model predictions in Figures 15 and 16. Figure 15 shows comparisons with the "no friction" mode run, while Figure 16 shows the same comparison with the "default" mode run that includes bottom friction. At the location of the alongshore groups of sensors PA3 to PA8, PV5-PV6, and PV1 to PV4, the *Hs* mean, maximum, and minimum values are shown to indicate the degree of alongshore variability.

Comparing the SWAN predictions from both the "no friction" and "default" runs with the observations, it is apparent that the "no friction" run tends to overpredict the wave heights at the inshore sites, whereas the "default" run does not show this bias and agrees better with the observations in a general sense. The exception to this pattern is Case 3, in which both the "no friction" and the "default" runs underpredict the wave height. Some of this small (<10%) error appears to be the result of not exactly matching the offshore wave condition at DW1, owing to errors in the discretization of the offshore boundary condition.

1. Cross-shore Transect

The observed cross-shore variation of the wave height *Hs* shows a general trend in all the case studies of wave decay from offshore to onshore, that is more pronounced in the onshore part of the array. It is most clearly seen in cases 2, 3, and 4, where the waves arrived at a moderate oblique incidence angle (25–32 degrees at the peak frequency). This can be explained by the

combined effect of refraction and bottom friction, with the former more dominant in these cases. Case 5, the most energetic one, also shows a wave decay trend from offshore to onshore (except for the *Hs* value at the PA2 site, which appears to be an outlier). In this case, the offshore wave field was coming in at a very small incidence angle (~1 degree) and the decay is mostly seen in the onshore part of the transect. A decay of about 15% of the incident wave height is observed at the inshore end of the transect in this case. Wave decay of the same order is also observed in cases 1, 2, and 4. In Case 3, the case with the shortest wave period, the observed and predicted wave decay is only about 5%, confirming that bottom effects (refraction and friction) are less important for shorter wavelength waves, that "feel the bottom" to a lesser degree than the longer period swells in the other case studies. These observed cross-shore wave decay rates agree fairly well with model predictions (using the "default" bottom friction setting) along the central transect of the array.

2. Alongshore Transects

The wave height observations *Hs* of the alongshore transects PA3 to PA8, PV5-PV6, and PV1 to PV4, show in some cases significant variability that is to a lesser degree also predicted by the SWAN model (Figures 15 and 16). This variability is most pronounced along the shallower transect (PV1 to PV4), and weaker along the deeper transect (PA3 to PA8).

Focusing on the shallower PV sites, in cases 2, 5, and 6 strong variability (15–30 %) is seen both in the observed and, to a lesser degree, predicted *Hs*. In Case 2, the least energetic, the observed *Hs* variability is comparable to that predicted by the model. In cases 5 and 6, where the waves are more energetic, the *Hs* mean values agree quite well but there is more alongshore variability in the observed *Hs*. The model-predicted wave height field for these case studies (Figure 12) shows a tongue-like feature of low values in the vicinity of the PV4 location. This tongue-like feature matches one of the trenches identified in the side-scan sonar image shown in Figure 14 (courtesy of Dr. Peter Traykovski,

Woods Hole Oceanographic Institution). The white colored patches in the image indicate deeper areas with coarser sand grains, also known as *Ripple-Scour Depressions*. The spatial pattern of the model-predicted wave height field closely resembles these cross-shore oriented bathymetry features (Figure 12). Observed and SWAN-predicted *Hs* variations along the PV1 to PV4 transect are shown in Figure 17 for Case 2. The stronger *Hs* decay at the PV4 site relative to the other sites is seen in the observations as well as in the predictions, and it is of about the same order. The trench in the vicinity of PV4 appears to play an important role in the wave decay at this site, and SWAN seems to handle quite well the combined effect of refraction and bottom friction in this low energy case.

In the energetic cases 5 and 6, however, strong alongshore wave height variability at the shallower PV sites is seen clearly in the observations, but to a lesser degree in the predictions. A possible explanation for this disagreement is the effect of sediment grain size on the bottom friction process, which is expected to be more important for energetic wave fields (Ardhuin et al., 2003). The alternating patches of coarse and fine sediments visible in the side-scan image (Figure 14) may cause heterogeneous wave decay that contributes to the observed alongshore *Hs* variability. This effect may also be the cause of the unexplained observed *Hs* variations at some PA sites (e.g., Case 5 on Figure 16). The SWAN bottom friction parameterizations do not account for differences in sediment size and thus do not predict this effect. Nevertheless, the mean observed and predicted *Hs* values agree fairly well in most cases, which indicates that SWAN predicts the main features of the observed wave evolution over the Martha's Vineyard inner continental shelf, while missing some of the small scale variations. A summary of the performance of SWAN with the different bottom friction parameterizations is given in the next section.

C. MODEL SKILL

With the purpose of evaluating the overall performance of SWAN against the observations across the nearly 4 km-long array transect, a scatter plot is

presented in Figure 18, that shows the predicted versus the observed wave height *Hs*. The predicted *Hs* are those obtained from the SWAN runs with the bottom settings shown in table 1 (not included are the “flat bottom” and the “no sources” modes). In addition to the scatter plot, two metric parameters are shown to evaluate the skill of the SWAN model in the six case studies. The first of them is the Bias (=$(\overline{Hs_{SWAN} - Hs_{OBS}})$) in units of meters, and the second one is the Root Mean Square (RMS) Error (=$\sqrt{\overline{(Hs_{SWAN} - Hs_{OBS})^2}}$), also in units of meters. The Bias is helpful to identify a model tendency to either *Hs* overestimation or underestimation, while the RMS Error quantifies in an absolute sense the accuracy of the predicted *Hs*. The scatter plot includes a total of 84 pairs (6 case studies x 14 sites) of observed and predicted *Hs* values. The cluster of data farthest to the right of the plot, well apart from the one-to-one correspondence line, corresponds to the comparisons at the PA2 site in Case 5, where the observed *Hs* is unusually large. These unexplained outliers were not included in the computations of the Bias and RMS Error.

The computed Bias values show that on average all the SWAN parameterizations neither overpredict nor underpredict significantly the *Hs* values, with the exception of the “friction 5” setting that slightly underpredicts (~ 4 cm) the wave height. The “no friction” setting, on the other hand, overpredicted the *Hs* values on average by about 3 cm. This result was expected, since the predicted wave decay without bottom friction should be less than with friction.

The RMS Error results show also a small difference between the “no friction” and the friction settings, with the former having the largest error value of 11 cm. The various friction settings yielded slightly improved RMS Error values between 9–10 cm.

Overall, these statistics show that all the bottom friction settings, including the widely used JONSWAP default setting, on average yield acceptable results across the array, and that deactivating friction in the model makes it perform slightly worse.

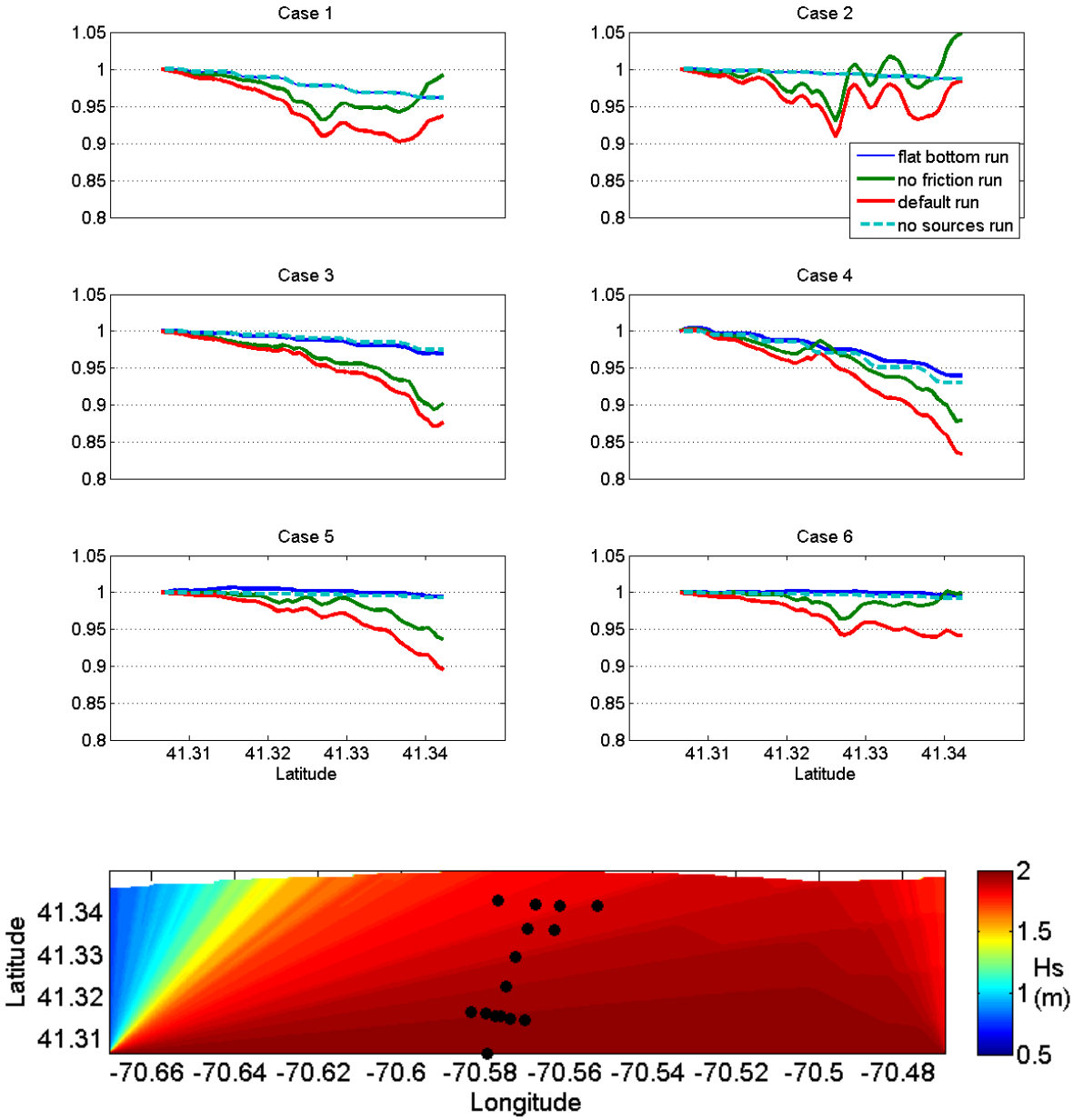

Figure 11. Predicted *Hs* variation with latitude across the central transect of the array connecting DW1 and PV2 (Top panel plots) for different SWAN mode runs. The *Hs* predictions are normalized by the *Hs* value at the DW1 site to show the relative wave height decay. Bottom panel shows the SWAN *Hs* output over the computational grid area for the "no sources" run in case 4.

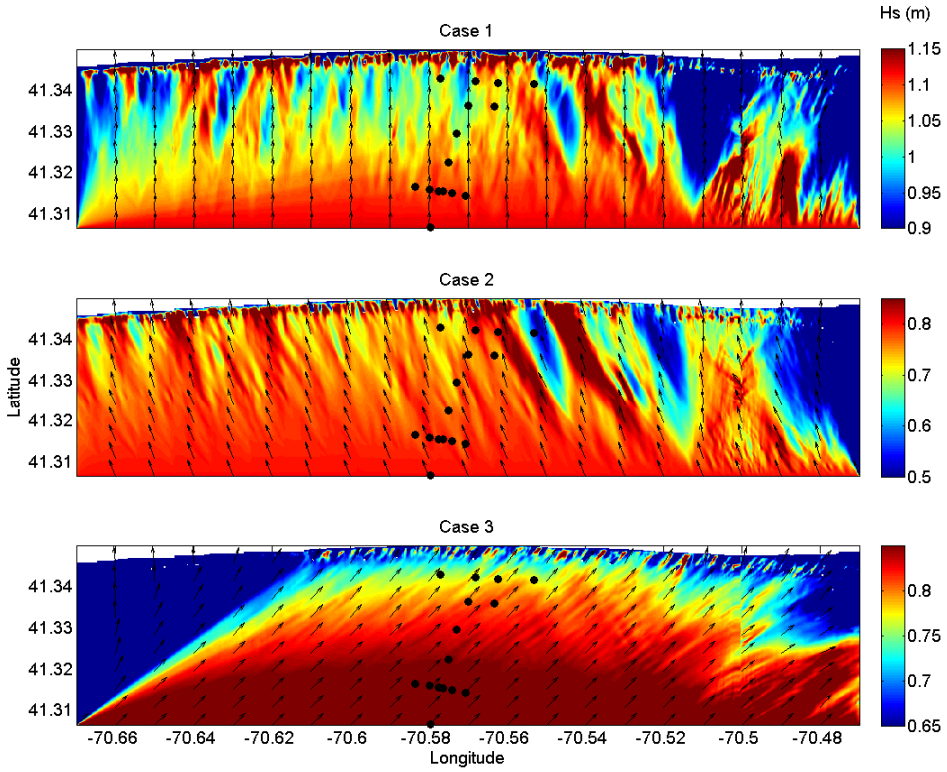

Figure 12. SWAN *Hs* output with mean directions at the peak period overlaid for cases 1, 2, 3. SWAN mode is "default." *Hs* variation throughout the computational grid area is sensitive to incoming wave mean direction, incident wave energy and bottom topography irregularities.

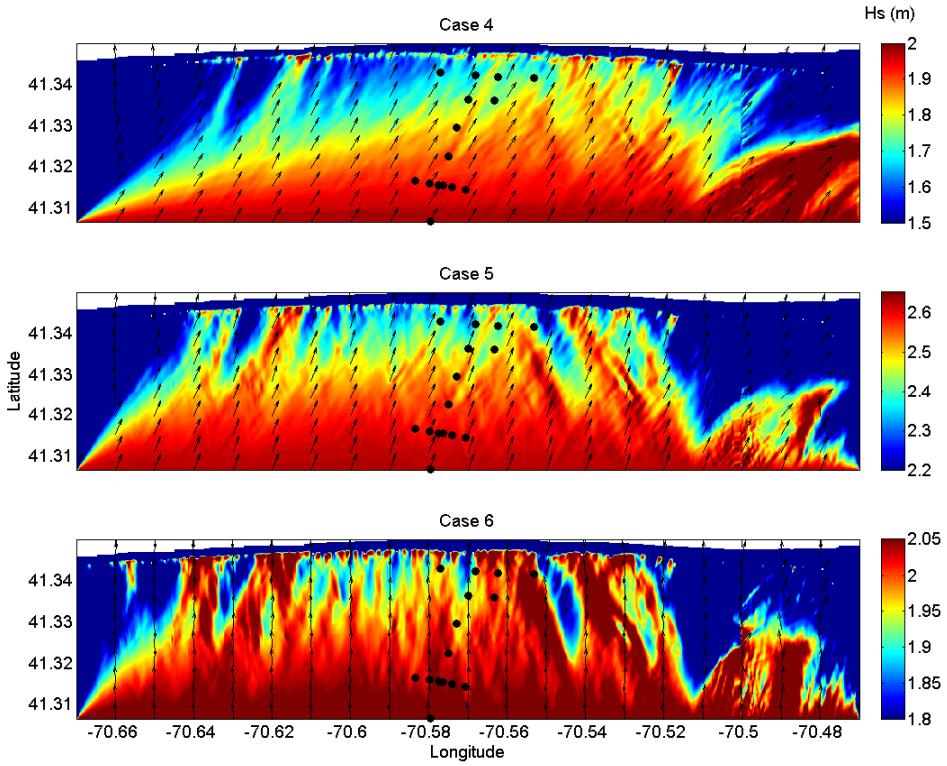

Figure 13. Same as figure 12 for cases 4, 5, and 6 (more energetic than the previous cases). In some cases, the wave height decay is of the order of 20% of the incident wave height.

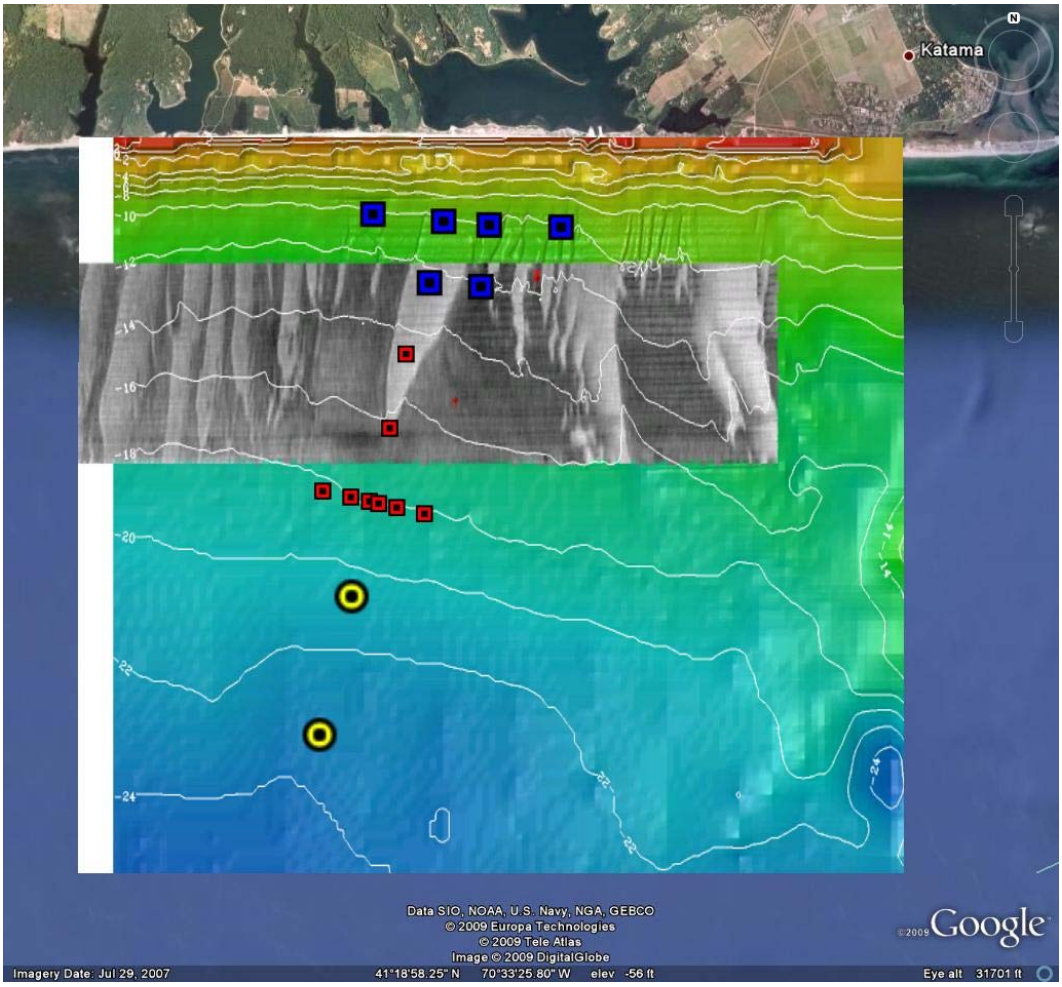

Figure 14. Google©2009 image with overlying side-scan sonar image and depth contours in the vicinity of the array of instruments. The white areas show trenches with coarser sand. Compare these features with the ones on figures 12 and 13. (Side-scan sonar image and bathymetry courtesy of Dr. Peter Traikovsky, Woods Hole Oceanographic Institution).

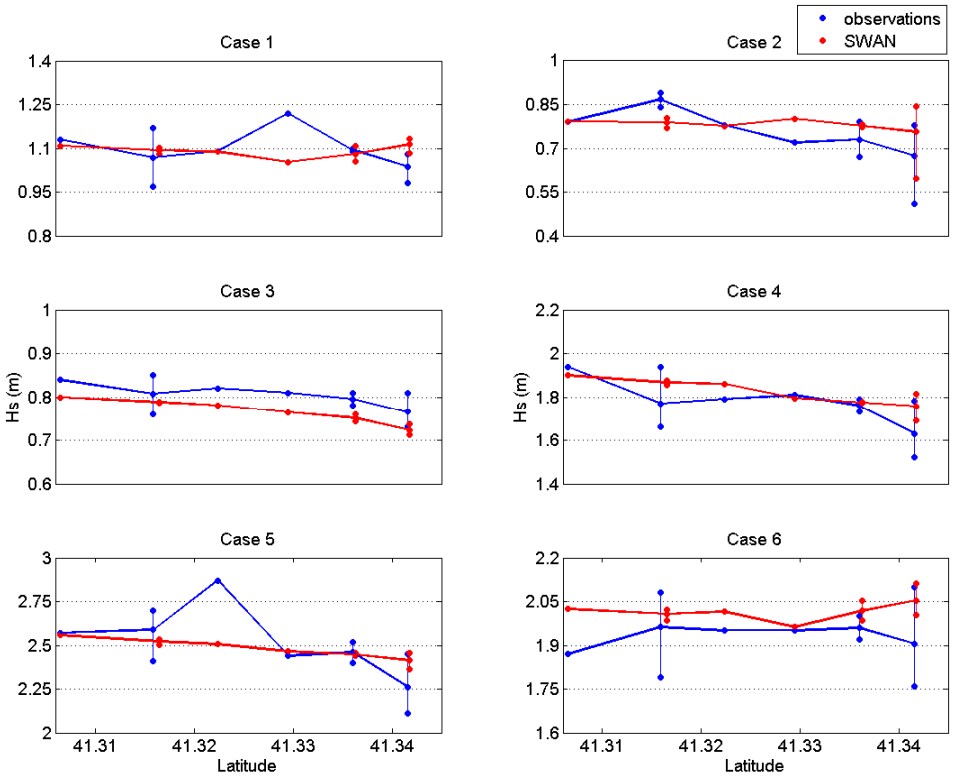

Figure 15. Comparison between the observed *Hs* across the array of instruments and the SWAN predicted *Hs* obtained with the "no friction" mode, for the six case studies. For the locations of the array where more than one instrument is present in the alongshore direction, the mean value, the maximum, and the minimum are plotted and connected with a line. In the cross-shore direction, thicker lines connect mean values.

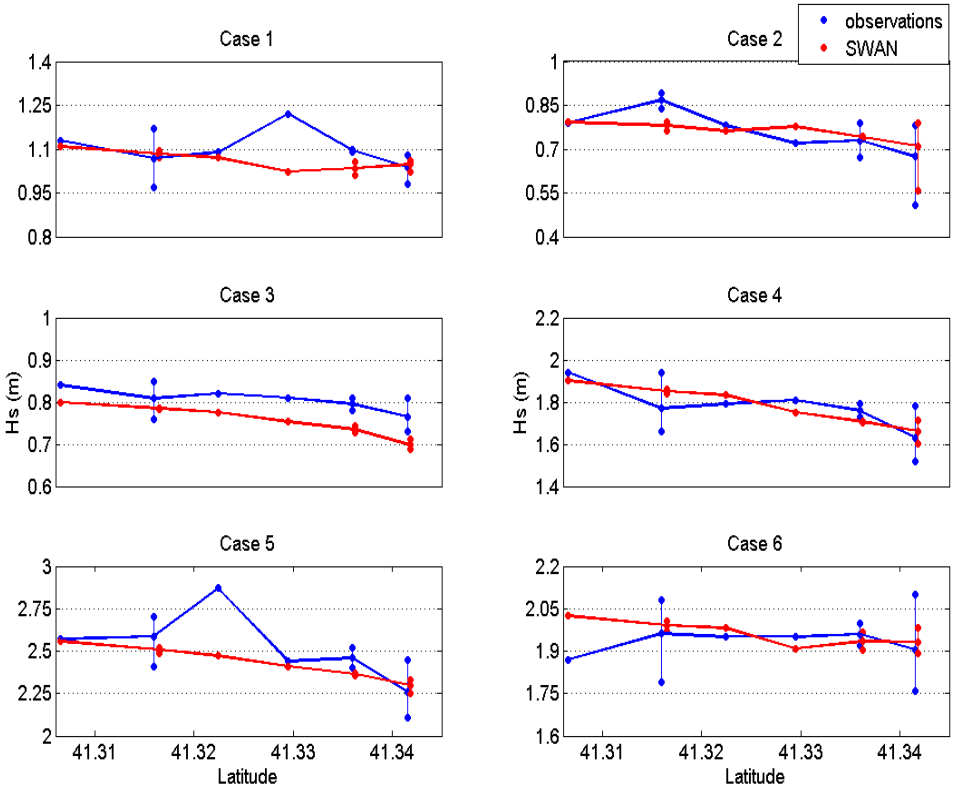

Figure 16. Same as figure 15, but SWAN "default" mode. The predicted *Hs* are smaller than those in figure 15, due to the activation of the bottom friction energy dissipation source.

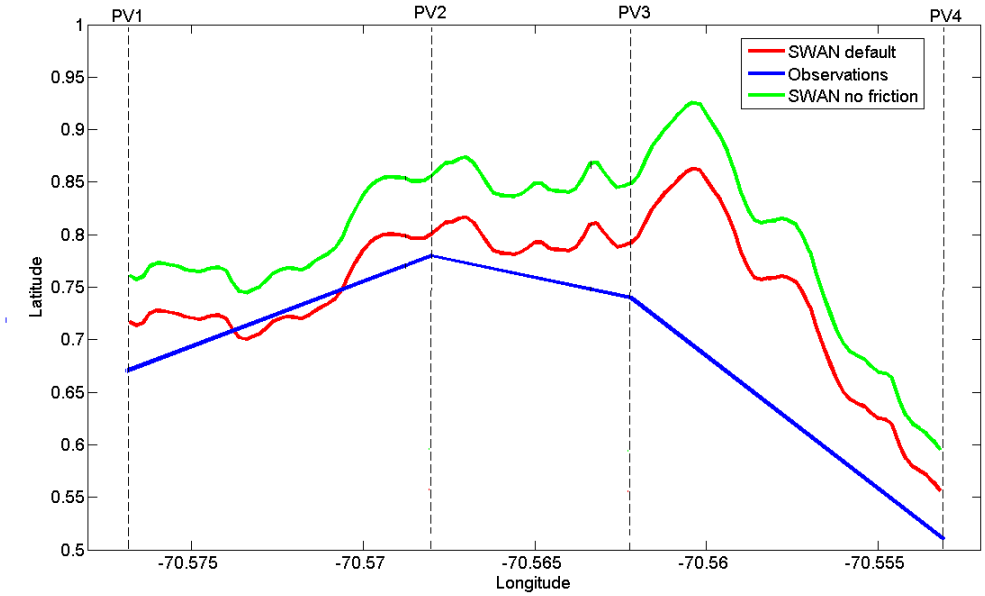

Figure 17. Alongshore cross-section of *Hs* predictions for case study 2, including the locations of the PV sensors closest to the shore. SWAN predicted *Hs* in "no friction" and "default" modes, and observed *Hs* at the four PV sites are shown. The common feature is the strong *Hs* decay at the PV4 site relative to the other PV sites resulting from refraction induced by a ripple-scour depression.

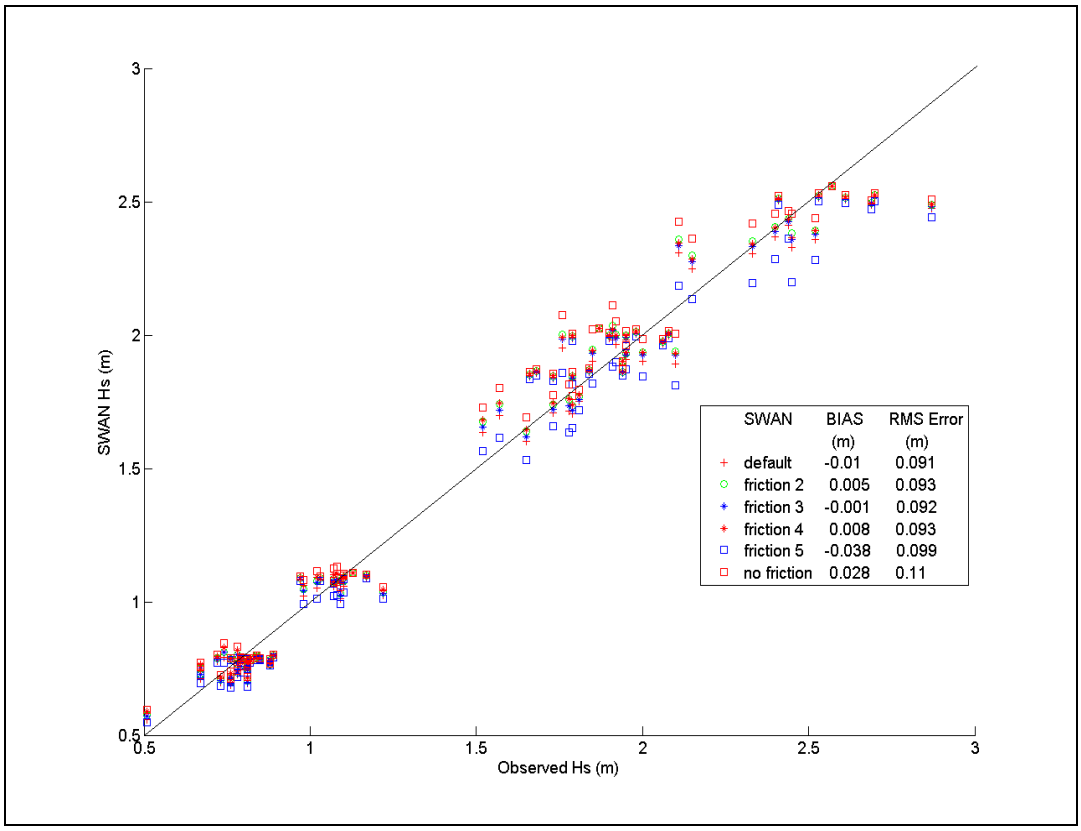

Figure 18. Scatter plot of SWAN-predicted versus observed *Hs*, for all the bottom friction parameterizations available in SWAN, estimated at the array sites with the complete data set corresponding to the six case studies. BIAS and RMS Error statistics are included in the legend. The solid diagonal line indicates a one-to-one correspondence.

VI. SUMMARY AND CONCLUSIONS

An extensive array of wave-measuring instruments was deployed for two months in 2007 on the inner continental shelf off the southern coast of Martha's Vineyard Island (Massachusetts), outside the surf zone. The observations taken from 16 instruments were analyzed and the wave evolution across the array was examined. The SWAN model was implemented in the area of the experiment to obtain wave predictions to be tested against the observations, and to isolate sources/sinks of wave energy. Since bottom friction was expected to be the dominant process in wave dissipation, the different parameterizations available in SWAN were applied. The two main objectives of this thesis are to determine what processes control wave evolution across the inner continental shelf over a sandy bed, and the evaluation of the performance of the widely used SWAN wave prediction model.

The first objective yielded the result that not only bottom friction but also refraction contributed to the evolution of wave energy in this experiment. The combined effect of the two processes resulted in observed and predicted wave height decay across the array of instruments of up to nearly 15% of the incident wave height. Wave height variability was observed both in the cross-shore and in the alongshore transects of the array, suggesting that the effect of refraction on wave energy is two-dimensional and very sensitive to small spatial changes in bottom topography. The presence of ripple-scour depressions with coarser sediments in the vicinity of the array contributes to the observed alongshore wave energy variability in two ways. Refraction induced by alongshore depth variations cause areas of energy convergence and divergence near the shore. Additionally, the alternating patches of coarse and fine sand may affect bottom friction decay rates that also contribute to alongshore wave energy variations. Whereas the refraction effect appears to be well described by the SWAN

predictions, the bottom friction parameterizations in SWAN do not account for heterogeneous sediment properties and thus the importance of this effect is not understood.

The second objective was achieved by running the model with the different bottom friction settings and comparing the results with the observations. The default bottom friction parameterization based on the JONSWAP study (Hasselmann et al., 1973) for fully developed wind sea conditions over shallow water, yielded predictions that agree well with the observed wave decay. However, the other bottom friction settings gave good overall results as well. The overall performance of the SWAN model in this case study is considered to be acceptable for most practical purposes including naval operations carried out in littoral areas.

Future research could include a more detailed study of the role played by the sand grain size in wave dissipation by bottom friction. Also, the results presented in this thesis refer to six selected case studies. A more complete model performance test could be carried out with a model hindcast of the entire two-month long experiment data set.

LIST OF REFERENCES

Ardhuin, F., Herbers T.H.C., and O'Reilly, W.C. (2001). A hybrid Eulerian-Lagrangian model for spectral wave evolution with applications to bottom friction on the continental shelf. *J. Phys. Oceanogr., 31,6*, 1498–1516.

Ardhuin, F., and Herbers, T.H.C. (2002). Bragg scattering of random surface gravity waves by irregular seabed topography, *J. Fluid. Mech., 451*, 1–33.

Ardhuin, F., et al. (2003). Swell transformation across the continental shelf. Part I: Attenuation and directional broadening. *J. Phys. Oceanogr., 33*, 1921–1939.

Battjes, J.A., and Janssen, J.P.F.M. (1978). Energy loss and set-up due to breaking of random waves, *Proc. 16th Conf. Coastal Engineering (Hamburg)*, New York, ASCE, pp. 569–587.

Battjes, J.A., and Stive, M.J.F. (1985). Calibration and verification of a dissipation model for random breaking waves, *J. Phys. Res., 90 (C5)*, 9159–9167.

Booij, N., Ris, R.C., and Holthuijsen, L.H. (1999). A third-generation wave model for coastal regions. 1. Model description and validation. *J. Geophys. Res. 104 (C4)*, 7469–7666.

Charnock, H. (1955). Wind stress over a water surface. *Quart. J. Roy. Meteorol. Soc. 81*, 639–640.

Collins, J.I. (1972). Prediction of shallow water spectra. *J. Geophys. Res. 77,* 2693–2707.

Dalrymple, R., and Liu, P. (1978). Waves over soft muds: A two-layer fluid model. *J. Phys. Oceanogr., 8*, 1121–1131.

Gade, H. (1958). Effectos of non-rigid, impermeable bottom on plane surface waves in shallow water. *J. Mar. Res., 16*, 61–82.

Hasselmann, K. (1962). On the non-linear energy transfer in a gravity-wave spectrum, part I: general theory. *J. Fluid Mech. 12,*.481.

Hasselmann, K., et al. (1973). Measurements of wind-wave growth and swell decay during the Joint North Sea Project (JONSWAP). *Dtsch. Hydrogr. Z. sup., A8(12)*, 95.

Herbers, T.H.C., Elgar, S., Guza, R.T. (1999). Directional spreading of waves in the nearshore. *J. Geophys. Res., 104(C4)*, 7683–7693.

Herbers, T.H.C., Hendrickson E.J., and O'Reilly W.C. (2000). Propagation of swell across a wide continental shelf, *J. Geophys. Res. 105 (C8),* 19729–19737.

Holthuijsen, L.H. (2007). Waves in Oceanic and Coastal Waters (1st ed). Cambridge University Press, New York.

Kantha, L.H., and Clayson, C.A. (2000). Numerical Models of Oceans and Oceanic Processes. Academic Press (San Diego).

Komen, G.J. Cavaleri, L., Donelan, M., Hasselmann, K., Hasselmann, S., and Janssen, P.A.E.M. (1994). *Dynamics and Modeling of Ocean Waves*. Cambridge University Press, New York.

Longuet-Higgins, M.S., Cartwright, D.E., and Smith, N.D. (1963). Observations of directional spectrum of sea waves using the motions of a floating buoy. In Ocean Wave Spectra, *Proceedings of a Conference*, Easton, Maryland, National Academy of Sciences, Prentice Hall, 111–136.

Lowe, R.J., et al. (2005). Spectral wave dissipation over a barrier reef. *J. Phys. Res., 100(C04001), doi:10.1029/2004JC002711*. 1–16.

Lygre, A., and Krogstad, H.E. (1986). Maximum entropy estimation of directional distribution in ocean wave spectra. *J. Phys. Oceanogr., 16*, 2052–2060.

Madsen, O.S., Poon, Y.,-K, and Graber, H.C. (1988). Spectral wave attenuation by bottom friction: theory, *Proc. 21st Int. Conf. Coastal Engineering (Malaga)*, New York, ASCE, pp. 492–504.

Miles, J.W. (1957). On the generation of surface waves by shear flows. *J. Fluid Mech. 3*, 185–204.

O'Reilly, W.C., Herbers, T.H.C., Seymour, R.J., and Guza, R.T.(1996). A comparison of direction buoy and fixed platform measurements of Pacific swell. *J. of Atmospheric and Oceanic Technology, 13(1)*, 231–238.

Phillips, O.M. (1957). On the generation of waves by turbulent wind. *J. Fluid Mech. 2*, 417–445.

Phillips, O.M. (1958). The equilibrium range in the spectrum of wind-generated water waves. *J. Fluid Mech. 4*, 426–434.

Pierson, W.J., Neumann, G., and James, R.W, (1955). *Practical Methods For Observing and Forecasting Ocean Waves by Means of Wave Spectra and Statistics,* Washington, U.S. Navy Hydrographic Office, Publication No. 603 (reprinted 1960).

The SWAN team (2009) SWAN Cycle III version 40.72AB User Manual, from http://www.fluidmechanics.tudelft.nl/swan/default.htm (accessed on 01/10/2009)

Thornton, E.B, and Guza, R.T. (1983). Transformation of wave height distribution, *J. Phys. Res., 88 (C10)*, 5925–5938.

Tolman, H.L., and Chalikov, D. (1996). Source terms in a third-generation wind-wave model. *J. Phys. Oceanogr., 26*, 2497–2518.

Trainor, L.T. (2009). Field Observations and SWAN model predictions of wave evolution in a muddy coastal environment. *Master Thesis*. Naval Postgraduate School (Monterey).

Traykovski, P., Hay, A.E., Irish, J.D., and Lynch, J.F. (1999). Geometry, migration, and evolution of wave orbital ripples at LEO-15. *J. Geophys. Res. 104(C1)*, 1505–1524.

WAMDI Group (1988). The WAM model–a third generation ocean wave prediction model. *J Phys. Oceanogr., 21*, 149–172.

Young, I.R., and Gorman, R.M. (1995). Measurements of the evolution of ocean wave spectra due to bottom friction. *J. Phys. Res., 100(C6)*, 10987–11004.

THIS PAGE INTENTIONALLY LEFT BLANK

INITIAL DISTRIBUTION LIST

1. Defense Technical Information Center
   Ft. Belvoir, Virginia

2. Dudley Knox Library
   Naval Postgraduate School
   Monterey, California

3. Professor T.H.C. Herbers, Department of Oceanography (Code OC/He)
   Naval Postgraduate School
   Monterey, California

4. Professor Jamie MacMahan, Department of Oceanography
   Naval Postgraduate School
   Monterey, California

5. Mr. Paul Jessen, Department of Oceanography
   Naval Postgraduate School
   Monterey, California

6. LCDR Guillermo Coll Florit
   Instituto Hidrografico de la Marina
   Cadiz, Spain